Sedimentary Geology
Manuscript Draft

Manuscript Number: SEDGEO5690

Title: Cave-fills in Miocene-Pliocene strata on Cayman Brac, British West Indies: Implications for the geological evolution of an isolated oceanic island

Article Type: Research Paper

Keywords: Cave; cave deposits; terra rossa; flowstone; karst

Abstract: An 8 m high wall in a quarry on the west end of Cayman Brac exposes the upper part of the Cayman Formation (Miocene), the lower part of the overlying Pedro Castle Formation (Pliocene), and the Cayman Unconformity, which a karstic unconformity that separates these formations. The modern-day karst surface caps the Pedro Castle Formation. This exposure also includes cross-sections through two filled caves - the "Lower Cave" (> 8 m long, up to 2.5 m high) and "Upper Cave" (>23 m long, up to 2 m high) that are housed in the Cayman Formation and Pedro Castle Formation, respectively.

The Lower Cave is filled with caymanite, which is formed of laminated, varicoloured dolomitized mudstones and grainstones that contain scattered marine fossils (e.g., foraminifera, red algae). This cave, connected to the Cayman Unconformity by a small-diameter tunnel, evolved as part of the karst system that developed during the Messinian lowstand. The cave was filled and dolomitized prior to deposition of the Pedro Castle Formation. The Upper Cave is filled with a wide spectrum of lithotypes, including dolostones, calcareous mudstones, terra rossa, gastropod coquina, coated grains, and speleothems. U/Th dating indicates that some of the flowstones are >500,000 years old whereas others are only ~ 21,000 years old. Dolostones and mudstones in the basal part of the Upper Cave contain marine fossils (foraminifera, red algae) whereas the younger deposits are devoid of such fossils.

The Upper Cave and its deposits developed after the sediments of the Pedro Castle Formation had been deposited and lithified. Development of the cave filling deposits, which includes a clear transition from marine to non-marine influences, was controlled by eustatic sea-level changes and/or westward tectonic tilting of Cayman Brac that occurred after the Pedro Castle Formation became exposed, probably during the Late Pliocene.

CAVE-FILLS IN MIOCENE–PLIOCENE STRATA ON CAYMAN BRAC, BRITISH WEST INDIES: IMPLICATIONS FOR THE GEOLOGICAL EVOLUTION OF AN ISOLATED OCEANIC ISLAND

Brian Jones

Department of Earth and Atmospheric Sciences, University of Alberta. Edmonton, Alberta, Canada, T6G 2E3

Key Words: Cave, cave deposits, terra rossa, flowstone, karst

Corresponding author: Brian Jones

E-mail address: Brian.Jones@ualberta.ca

ABSTRACT

An 8 m high wall in a quarry on the west end of Cayman Brac exposes the upper part of the Cayman Formation (Miocene), the lower part of the overlying Pedro Castle Formation (Pliocene), and the Cayman Unconformity, which a karstic unconformity that separates these formations. The modern-day karst surface caps the Pedro Castle Formation. This exposure also includes cross-sections through two filled caves – the "Lower Cave" (> 8 m long, up to 2.5 m high) and "Upper Cave" (>23 m long, up to 2 m high) that are housed in the Cayman Formation and Pedro Castle Formation, respectively.

The Lower Cave is filled with caymanite, which is formed of laminated, varicoloured dolomitized mudstones and grainstones that contain scattered marine fossils (e.g., foraminifera, red algae). This cave, connected to the Cayman Unconformity by a small-diameter tunnel, evolved as part of the karst system that developed during the Messinian lowstand. The cave was filled and dolomitized prior to deposition of the Pedro Castle Formation. The Upper Cave is filled with a wide spectrum of lithotypes, including dolostones, calcareous mudstones, terra rossa, gastropod coquina, coated grains, and speleothems. U/Th dating indicates that some of the flowstones are >500,000 years old whereas others are only ~ 21,000 years old. Dolostones and mudstones in the basal part of the Upper Cave contain marine fossils (foraminifera, red algae) whereas the younger deposits are devoid of such fossils.

The Upper Cave and its deposits developed after the sediments of the Pedro Castle Formation had been deposited and lithified. Development of the cave filling deposits, which includes a clear transition from marine to non-marine influences, was controlled by eustatic sea-level changes and/or westward tectonic tilting of Cayman Brac that occurred after the Pedro Castle Formation became exposed, probably during the Late Pliocene.

1. Introduction

Isolated oceanic islands, like the Cayman Islands, are commonly formed of unconformity-bounded limestone/dolostone sequences that formed in response to oscillating sea levels (e.g., Esteban and Klappa, 1983; Mylroie and Carew, 1995; Choquette and James, 1998; Liang and Jones, 2014). Although the unconformities in these successions may represent long periods of time it is commonly difficult to obtain information about the processes that were operative during those periods, largely because erosion and substrate modification predominate (e.g., Clari et al., 1995; Hillgartner, 1998; Sattler et al., 2005; Alonso-Zarza and Wright, 2010; Liang and Jones, 2015b). Joints, sinkholes, caves, and cavities, which are integral components of karst terrains, become receptacles where sediments can be deposited and speleothems precipitated (Jones and Smith, 1988; Jones, 1992b). Such deposits " . . . are of great importance, because once formed they are more protected from subsequent erosion than the contemporaneous surface sediments. They may thus preserve sediments and faunal remains for periods from which all other records are lacking" (Smart et al., 1988, p. 159). Sediments that accumulate in caves may come from multiple sources (e.g., Fornós et al., 2009, their Fig. 13; Farrant and Smart, 2011; van Hengstum and Scott, 2012; Fornós et al., 2014, their Fig. 10) and therefore have the potential of yielding information about the surface processes that were ongoing while the islands were exposed to the atmosphere.

This study focuses on a Miocene–Pliocene succession that is well exposed in the West End Quarry on Cayman Brac (Fig. 1). There, the quarry walls (up to 8 m high) include excellent exposures of the upper part of the Cayman Formation (Miocene), the Pedro Castle Formation (Pliocene), and two unconformities. The Cayman Unconformity is the boundary between the two formations (Jones and Hunter, 1994b) whereas the top of the quarry wall is the modern karst surface that caps the Pedro Castle Formation (Fig. 2). The east wall of the quarry includes exposure of (1) a filled cave in the Cayman Formation that developed in association with the Cayman Unconformity and predated deposition of the Pedro Castle Formation, (2) a filled cave in the Pedro Castle Formation that postdated deposition of that formation, and (3) filled cavities that crosscut the Pedro Castle Formation and the Cayman Formation and parts of the filled caves.

Although numerous studies of cave-filling deposits have been presented (e.g., Ginés et al., 1981; Goodfriend and Mitterer, 1993; Foos et al., 2000; Cowie and Grant-Mackie, 2004; Ginés and Ginés, 2007; Auler et al., 2009; Fornós et al., 2009; Farrant and Smart, 2011; Martini, 2011; van Hengstum et al., 2011; Iacoviello and Martini, 2012; van Hengstum and Scott, 2012; Iacoviello and Martini, 2013; Fornós et al., 2014), little attempt has been made to integrate that information with the development of the bedrock succession that house the caves. Accordingly, this study, using the succession on Cayman Brac as an example, demonstrates the advantages of integrating the paragenetic histories of the bedrock succession and the cave-filling deposits for determining the geological evolution of an isolated island. In particular, such an analysis provides information on the processes that were operative during sea level lowstands when the island was exposed and karst and soils were developing under subaerial conditions.

2. Geological setting

Cayman Brac is a small, isolated island surrounded by deep waters of the Caribbean Sea (Fig. 1A). The elevated core of the island, which slopes westward from ~ 40 m above sea level (asl) at its east end to sea level at its west end, is skirted by a low-lying platform that is 2-3 m asl (Fig. 1B, C). The core of the island is formed of limestones and dolostones that belong to the Bluff Group (Fig. 2) whereas the peripheral platform is formed of limestones that belong to the Ironshore Formation (Fig. 1B).

This study is based an exposure in the West End Quarry (SQA), which is an actively producing quarry located on the west end of Cayman Brac (Fig. 1B). The quarry walls, 6 to 8 m high, provide excellent sections through the upper part of the Cayman Formation (Miocene), the lower part of the Pedro Castle Formation (Pliocene), and the Cayman Unconformity (Fig. 3). The pervasively dolomitized Cayman Formation is characterized by skeletal wackestones/packstones that contain numerous massive (e.g., *Porites*, *Diploria*, *Montastrea*, *Favia*) and branching (e.g., *Stylophora*, *Porites*) corals along with red algae, bivalves, and gastropods (MacNeil and Jones, 2003). The Pedro Castle Formation is formed largely of skeletal wackestones that are characterized by foraminifera, red algae, branching corals (*Stylophora*, *Porites*) and scattered massive (*Montastrea*) corals (MacNeil and Jones, 2003). On this part of the island, the basal 0.5 to 1.0 m of the Pedro Castle Formation is formed of dolostone that is overlain by dolomitic limestone that is, in turn, overlain by limestone (Jones, 1994; Jones and Hunter, 1994a; MacNeil and Jones, 2003). Two unconformities are evident in this quarry wall. The Cayman Unconformity developed during the Messinian lowstand (Jones and Hunter, 1994b; Liang and Jones, 2015a), whereas the other unconformity, 3 to 4 m above the Cayman Unconformity, is the present day karst surface that is characterized by a rugged karst landscape (Liang and Jones, 2014).

3. Methods

The stratigraphic succession, location of the Cayman Unconformity, and the caves were mapped in the field. For ease of reference the filled caves in the Cayman Formation and Pedro Castle Formation are herein called the "Lower Cave" and "Upper Cave" respectively.

Orientated samples were collected from the bedrock and all of the cave-filling deposits. The basic petrography of the rocks was established from 16 large (7 x 5) and 7 small thin sections (4.5 x 2.5 cm) made from samples impregnated with blue epoxy. Thin sections were stained with Alizarin Red S solution in order to separate the calcite from the dolomite.

The mineralogy of each sample was confirmed by X-ray diffraction analysis. Powdered samples, each weighing ~ 1 g, were analyzed on a Rigaku Ultima IV Powder X-ray system that was run at 38 kV and 38 mA using an Ultima IV X-ray generator with a Co tube. All scans were run from 5 to 90° 2Θ at a speed of 2° Θ/min. Mineral identifications were derived using the JADE 9.5 computer program that operates in tandem with the X-ray system.

Selected samples were examined on a Zeiss Sigma 300 VP-FESEM scanning electron microscope (SEM) that can be operated under high vacuum and variable pressure. Samples examined on the SEM included (1) fractured samples, up to 3 cm^3, that were broken off the parent sample, (2) small and large uncovered thin sections, (3) rock slices, up to 4 x 4 x 0.5 cm, cut from a sample and polished on one surface, or (4) small samples (~ 1 cm^2) with micro-milled surfaces that were prepared using a Fischione SEM Mill Model 1060 using 4kV and 50% focus with the sources positioned to four degrees and the sample continuously rotated.

Some samples examined on the SEM were left uncoated whereas others were coated with carbon. Images were obtained under variable conditions that depended on the sample. Some images are in normal mode whereas others are backscattered electron (BSE) images. Spot analyses, line transects, and elemental maps were obtained using a high resolution Bruker dual detector for energy-dispersive X-ray spectroscopy (EDS) system that is attached to the SEM. These standard-less, semi-quantitative analyses must be treated with caution given that the weight-percent values are probably ±5%. Accordingly, these data were used largely to delineate trends and major changes in elemental contents that are apparent along transect lines or from the comparison between different points.

$^{87}Sr/^{86}Sr$ ratios were obtained for four samples of dolostone in the Radiogenic Isotope Laboratory at the University of Alberta using the procedures described by MacNeil and Jones (2003). These analyses supplemented the analyses reported in MacNeil and Jones (2003) and Zhao and Jones (2012). All data were normalized to SRM 987 (0.710245). The error margin for these analyses is $\pm$ 0.00002.

Twenty O^{18} and C^{13} isotope analyses, done by Isotope Tracer Technologies Inc. (Waterloo, Canada), were obtained using a DELTA^{Plus} XL Stable Isotope Ratio Mass Spectrometer (IRMS) that is coupled with a ConFlo III interface and EA1110 Elemental Analyzer. All results are reported against the Vienna Peedee Belemnite (VPDB). Standards were run before, during, and after analysis of the samples in order to maintain accuracy. The error margin for the O^{18} and C^{13} is $\pm$ 0.1‰. These analyses supplement the analyses reported by MacNeil and Jones (2003) and Zhao and Jones (2012).

Three samples of flowstone were subject to U/Th dating. These analyses were analyzed by Dr. Bassam Ghaleb induction-coupled mass spectrometry (ICPMS) at GEOTOP, Montreal, Quebec. These samples had low U concentrations and traces of ^{232}Th, which indicates that detrital material had been incorporated into the precipitated calcite. Thus, the calculated ages were corrected for this using the methodology of Ludwig and Paces (2002).

3. Terminology

Caymanite, named after local artisans who use it to make jewellery, is a multicoloured (white, red, black) finely crystalline dolostone with laminae that dip at angles up to 60° (Jones, 1992a). This cavity-filling internal sediment is common in the Cayman Formation. Although mentioned by Folk and McBride (1976), Rigby and Roberts (1976), and Lockhart (1986), it was examined in detail by Jones (1992a).

The term limpid dolomite, following Folk and Siedlecka (1974), Folk and Land (1975), Longman and Mench (1978), and Kaldi and Gidman (1982), is applied to water-clear dolomite crystals that commonly formed as a cement.

The term “terra rossa”, first used by Tućan (1912) for the distinctive red soils found in the Mediterranean region. Merino and Banerjee (2008, p. 62) stated that terra rossa, known from many areas throughout the world, are “… red claystones up to several metres thick and kilometers across that occur at the earth’s surface and are associated with karst carbonates”. In some areas, including Jamaica and France, terra rossa grades into bauxite (Merino and Banerjee, 2008). According to Durn et al. (1999), terra rossa is typically formed of quartz, plagioclase, K-feldspar, micaceous clay minerals, kaolinites, chlorite, vermiculite, smectite, hematite, goethite, XRD-amorphous inorganic compounds, and in some cases, calcite, dolomite, and boehmite. Bauxite is typically formed of gibbsite ($(Al(OH)_3)$, amorphous Al hydroxides, boehmite (γ $AlO(OH)$), diaspose (α $AlO(OH)$), hematite (Fe_2O_3), goethite ($FeO(OH)$), anatose (TiO_2), and kaolinite ($Al_2Si_2O_5(OH)_4$) (Boni et al., 2013).

Dolostones from the bedrock and the caves are divided into low-Ca calcium dolomite (LCD) that contains < 55 mol % $CaCO_3$ and high-Ca calcium dolomite (HCD) that contains >55 mol % $CaCO_3$ (Jones et al., 2001). Following the convention adopted by Jones et al. (2001), the mol % $CaCO_3$ is abbreviated to %Ca.

4. Results

4.1. Cave morphologies

The north-south oriented wall on the east side of West End Quarry has its base at 1.5 m, the Cayman Unconformity at 4.5 to 5.0 m, and its top at 7.5 m above sea level (asl). This quarry wall includes sections through the Lower Cave and the Upper Cave (Fig. 4). Late stage cavities cross-cut both caves and the bedrock.

The Lower Cave, which has an irregular cross-sectional shape, is at least 8 m long (south end is covered) with a maximum height of 2.5 m (Fig. 4A). At its north end, this cave appears to be connected to the Cayman Unconformity by a small-diameter (< 0.5 m) tunnel, but poor outcrop conditions in that area precluded a definitive assessment.

The Upper Cave, with an irregular cross-sectional morphology, is at least 23 m long and up to 2 m high (Fig. 4B). The north end of the cave is poorly exposed and impossible to map in detail. This cave may be formed of two or three smaller chambers that are linked together by short tunnels, but poor outcrop conditions in this critical area prevented resolution of this issue. Although the base of the cave is typically coincident with or just above the Cayman Unconformity, it locally cuts down in the upper part of the Cayman Formation (Fig. 4B).

Small-diameter (< 2 m) subvertical sinkholes, located at the south end, the middle part, and possibly the north end of the exposure, extend down from the present-day surface (Fig. 4). The "Middle Sinkhole" intersects the Upper Cave (Fig. 4B), whereas the "South sinkhole" intersects the Upper Cave with parts extending down into the Lower Cave (Fig. 4A).

4.2. Lithotypes

The dominant lithotypes in the caves, based on field appearance and thin section analyses, are caymanite, finely crystalline dolostone, varicoloured calcareous mudstones, red terra rossa, red terra rossa breccia, terra rossa ooids, olive terra rossa, gastropod coquina, coated grains, and speleothems (Figs. 5-7).

4.2.1. Caymanite

Caymanite, restricted to the Lower Cave and small cavities in the dolostones of the Cayman Formation, is formed largely of white laminae and fewer, thin light to dark red and light grey laminae that dip at angles up to 60° (Fig. 4, 5). The caymanite is formed of very hard, dense HCD (56.7–57.3%Ca) that is composed of interlocking euhedral to subhedral crystals < 5 μm long (Figs. 8, 9). Although dominated by mudstone laminae, there are rare (< 1 cm thick) grainstone laminae that include fragments of red algae, small benthic foraminifera, planktonic foraminifera, and other unknown biofragments (Fig. 8). Some grainstone laminae include angular grains (< 1 mm long) of finely crystalline dolostone that were probably derived from the Cayman Formation (Fig. 8B). Some caymanite, especially in the upper part of the cave, contain pores (< 1 mm) lined with limpid dolomite cement and occluded by calcite cement (Fig. 9B).

4.2.2. Finely crystalline dolostone

Units A and B that form the basal part of the succession in the Upper Cave are finely crystalline dolostones (Fig. 6A). Unit A (20 cm thick) is white with vaguely defined laminae in the upper part, whereas unit B is characterized by off-white to very light pink horizontal laminae (Fig. 6A). They differ from caymanite because they (1) lack the multicolored laminae that dip at various angles, and (2) are “softer” and lack the porcellaneous appearance of caymanite.

The dolostone in Unit A, formed of subhedral to euhedral HCD (56.1 %Ca) crystals < 2 μm long (Fig. 10A-C), contains scattered dolomitized fragments of red algae (Fig. 10C). Small pores in the dolostone are lined with limpid dolomite cement and occluded by calcite (Fig. 10A).

The dolostone in unit B is formed of euhedral HCD (57.8 %Ca) crystals < 5 μm long (Fig. 10D-F). It contains scattered dolomitized red algae fragments and pores lined with limpid dolomite cement and filled with calcite. Unlike unit A, hollow dolomite crystals are common in the upper part of this unit (Fig. 10F).

4.2.3. Calcareous mudstone

The white to pink to red calcareous mudstones (Unit C, Fig. 6A, B, C), which overlie the dolostones of units A and B in the Upper Cave, are formed of anhedral to subhedral calcite crystals that are < 2 μm long with most being < 1 μm long (Fig. 11, 12A-C). No dolomite was detected in these mudstones. Some of the mudstones contain scattered foraminifera that are up to 0.5 mm long (Fig. 11C, D). The mudstones, typically forming beds < 2 cm thick, are structureless or finely laminated with graded bedding (Fig. 11B). Some of the mudstone beds show evidence of desiccation, brecciation, and clast rotation (Fig. 11E, F).

Pores and irregular fractures in the mudstones are lined or filled with calcite cement (Fig. 11A). No limpid dolomite cement was found. Larger cavities commonly have small lithoclasts on their floors that were then buried by mudstone, which were, in turn, coated by calcite cement (Fig. 11F). Many of the larger cavities were not completely filled.

All of the mudstones, which range from white to off-white to pink to red (Fig. 11A, B, C), contain scattered Fe-rich, ovate to spherical masses, that are up to 20 μm (typically < 10 μm) in diameter (Fig. 12D-L). The red mudstones have the highest concentration of Fe-masses whereas the white mudstones have the lowest. The microstructure of these Fe-rich masses ranges from triangular-shaped "crystals" (Fig. 11G) to "plates" (Fig. 11F) to structureless masses (Fig. 11I). EDS analyses show that they contain Fe (62-67%), O (27-30%), Al (2-4%), Si (1-2%), and Ca (1-3%) whereas the platy crystals contain 47% Fe (Fig. 13). The Ca is probably derived from minute particles of the matrix that are embedded in the Fe-rich precipitates.

4.2.4. Red terra rossa

The colour contrast between the red lithified terra rossa and the white dolostones of the bedrock makes it the most obvious deposit in the caves (Figs. 4, 5D, 6B, E). XRD analyses shows that it is formed of calcite, boehmite, gibbsite, anatase, and minor amounts of kaolinite. The calcite, however, is restricted to cobweb-like arrays of microfractures, typically < 0.1 mm wide, that radiate throughout the terra rossa (Fig. 14). Element maps emphasize the spatial discrimination with the ~~Ai~~, Si, Fe and other allied elements being restricted to irregularly shaped masses, typically < 0.5 mm long, that are surrounded by the calcite-filled fractures (Fig. 14D-F, 15). There is commonly more than one generation of calcite cement (Fig. 14G-I). In these cases, the larger masses of terra rossa are cut by microfractures that are filled with fibrous calcite that in plane polarized light is off-white to yellowish in colour (Fig. 14G, I). In contrast, the wider fractures around the larger masses are filled with calcite that is colourless in plane polarized light (Fig. 14G, I). Textural evidence indicates that this calcite formed after the off-white to yellowish calcite. EDS transects clearly highlight the compositional contrasts between the red terra rossa and the calcite (Figs. 14H, 15).

Red terra rossa imaged by standard SEM analyses of fractured and polished surfaces, appears amorphous and EDS spot and line analyses show that it is formed largely of Al, Fe, and Si (Fig. 15). Imaging and backscatter electron imaging of highly polished micro-milled samples, however, showed that the terra rossa has the following characteristics.

- The terra rossa is formed largely of lath- to plate-shaped crystals < 2 μm long and 250 nm wide but mostly < 250 nm long and < 100 nm wide (Figs. 16A-C). EDS analyses show that they are formed of Al and Si but do not contain Fe. Although compositionally consistent with boehmite and gibbsite (as identified by XRD analysis) it proved impossible to precisely identify which crystals are which minerals.

- The Fe is located in Fe-rich masses, < 5 μm in diameter (rare), and irregular-shaped grains, < 1 μm long and commonly < 100 nm long, that are randomly disseminated throughout the rock. These grains are assumed to be Fe-oxides because EDS failed to detect S in any of them. There is no obvious pattern to the distribution of the Fe.
- Throughout the terra rossa there are scattered exotic crystals/grains that are formed of (a) zirconium silicate, < 12 μm long (Fig. 16F), (b) Ti-oxides, < 15 μm long (Fig. 16G), (c) Cr and Fe (Fig. 16H) grains < 25 μm long, and (d) P, Ce, and La grains < 5 μm long (Fig. 16I). There is no obvious distribution pattern to these grains.

4.2.5. Terra rossa breccia

This distinctive rock, common in the upper part of the Upper Cave near the Middle Sinkhole, is formed of (1) irregular-shaped masses of red terra rossa up to 15 cm long and 10 cm high, (2) thinly laminated flowstone (up to 1 cm thick) that coats the terra rossa masses (Fig. 7C), and (3) calcareous mudstone that filled the areas between the flowstone (Fig. 7C). Irregular-shaped cavities, up to 5 cm high and wide, occur where the spaces between the terra rossa masses was not completely filled with flowstone and/or limestone (Figs. 7A, B).

Thin sections viewed in plane polarized light show terra rossa that is dark red to orange to yellowish brown in colour and dissected by irregular networks of calcite-filled fractures (Fig. 17A). BSE images and EDS analyses, however, failed to show any obvious compositional differences between the different colours of terra rossa (Fig. 17B, C, 18). Likewise, there was no obvious difference in the amount and distribution of disseminated Fe in these areas (Fig. 17D, E).

4.2.6. Terra rossa ooids

This lithotype comprises spherical to ellipsoidal ooids, up to 1 mm long, formed of red terra rossa held in spar calcite cement (Fig. 21). Although superficially uniform, these ooids are characterized by variable colours (as seen in plane polarized light), internal structures, and compositions (Figs. 21, 22). With plane polarized light, the ooids range from dark red to light reddish-orange (Fig. 21). Some are homogeneous with no apparent nucleus (Fig. 21A), whereas other ooids have a nucleus encased by a thin cortex (Fig. 21C) or a cortex that is irregular in thickness with multiple bands (Fig. 21E, G, I, K). Most nuclei are formed of terra rossa that appears denser and darker in colour relative to the surrounding cortex (Fig. 21E, J, L). In rare examples, small pieces of limestone form the nuclei (Fig. 21G).

BSE images and EDS analyses of the ooids show that, irrespective or colour, they are formed largely of Al, Si, and Fe with lesser amounts of Ca (Fig. 22). The lighter coloured cortical laminae, where present, reflect zones where Al, Si, Fe, and Ca mixed together in varying proportions (Fig. 22B, C, D, E, F). High magnification BSE images confirm that such zones are formed of interspersed calcite, clays, and Fe-oxide grains.

4.2.7. Olive terra rossa

The olive terra rossa fills cavities that crosscut the caves and/or cavities that are filled with red terra rossa (Fig. 6E). The olive terra rossa is cut by honeycombed arrays of calcite-filled microfractures (Fig. 17D, E). Under plane polarized light this terra rossa ranges from light- to dark-yellow brown to bright red with no readily discernable pattern (Fig. 19A). The colours evident under plane polarized light are deceptive because there are no obvious correlations between the colours and elemental content as revealed by EDS analyses (Fig. 2). Some of the bright red areas, for example, have a high Ca but low Al-Fe-Si content (Figs. 19C, 20A) whereas some of the brown-coloured areas have subequal amounts of Ca and Al-Fe-Si (Fig. 19E, 20B). Some of these “coloured” areas, like those shown in Figure 19B and 19C, are formed of small, irregular-shaped patches of clays and Fe that are scattered throughout a finely crystalline calcite groundmass. Thus, it is possible that the colour may, in some way, reflect the amount of calcite that is mixed in with the clays and Fe.

4.2.8. Gastropod coquina

Found only in one small area in the uppermost part of the Upper Cave north of the Middle Sinkhole (Fig. 4B), this lithotype is characterized by numerous, closely packed gastropods that are up to 1.5 cm high and 1.5 cm in diameter (Fig. 7F). The gastropods are well preserved with no evidence of alteration of their aragonitic shells. In most cases, however, the shells have been dislodged (probably during quarrying) and impressions are all that remain (Fig. 7F). Although the species is unknown, this appears to be a monospecific assemble of gastropods.

4.2.9. Coated grains

Coated grains, held in spar calcite cement, forms the (1) matrix between the gastropods in the gastropod coquina, and (2) bed that overlies the gastropod coquina. Up to 4 mm long, the ~~coasted~~ grains have various types of nuclei that are encased by cortical laminae formed of micrite that commonly contains small shell fragments (Fig. 23). Nuclei range from complete gastropod shells (Fig. 23A, B) to fragments of gastropod shells (Fig. 23C-E), to small limestone fragments (Fig. 23F). Some body cavities in the gastropods are partly filled with terra rossa ooids (< 1 mm diameter) and/or spar calcite cement (Fig. 23B). Vague laminations in the cortices are defined by subtle differences in colour (Fig. 23E, F). The oncoids are typically coated with a thin isopachous rind of calcite cement ~~(Fig. 13 D).~~ Pores between the oncoids are filled with terra rossa ooids, small shell fragments, and spar calcite cement (Fig. 23).

Despite careful examination of the oncoids at high magnifications on the SEM, no evidence of microbes was found in their ~~cortices,~~

4.2.10. Speleothems

Speleothems in the Upper Cave include flowstone (Fig. 6E), stalactites and draperies (Fig. 7D, E), and rare stalagmites. No speleothems were found in the Lower Cave.

In the lower part of the Upper Cave, brownish flowstone (up to 15 cm thick) is intercalated with the white to red mudstones (Fig. 6E) and, in some areas, thin beds of red terra rossa. The banded flowstone is formed largely of densely packed prismatic calcite crystals that are up to 2 cm long and 5 mm wide. Exceptions to this motif include (1) laminae formed of small dendritic bushes, and (2) thin brown to dark grey micrite laminae that have a pseudo-stromatolitic appearance. No evidence of microbes was detected in these layers. There is no textural evidence to indicate that the calcite formed through alteration of aragonite.

The flowstone in the upper part of the cave, which coats the terra rossa, is thinly laminated and lacks the distinctive brownish colour of the lower flowstone (Fig. 7C).

Stalactites and draperies adorn the cave ceiling where the cave was not completely filled by sediments and flowstone (Fig. 7D, E). The stalactites and draperies, up to 15 cm long, are distinctive because of their surface white color (Fig. 7D, E). Sections through the stalactites and draperies show that they are thinly laminated and formed entirely of calcite.

Rare stalagmites, found only in the area below the Middle Sinkhole, are poorly developed and no more than 6 cm high and 5 cm in diameter.

4.3. $^{87}Sr/^{86}Sr$ ratios

Dolostones in the upper part of the Cayman Formation have $^{87}Sr/^{86}Sr$ ratios of 0.70902 to 0.70913 (Zhao and Jones, 2012) whereas the dolostones in the Pedro Castle Formation have $^{87}Sr/^{86}Sr$ ratios of 0.70903 to 0.70911 (MacNeil and Jones, 2003).

Additional $^{87}Sr/^{86}Sr$ ratios obtained during this study include values of (1) 0.70905 ± 0.00003 for dolostone from the Cayman Formation beside the Lower Cave, (2) 0.70907 ± 0.00003 for the caymanite in the Lower Cave, (3) 0.70907 ± 0.00002 for the dolostone in Unit A of the Upper Cave, and (4) 0.70913 ± 0.00004 for the dolostones in Unit B of the Upper Cave (Fig. 24).

4.4. Carbon and oxygen stable isotopes

According to Zhao and Jones (2012), dolostones in the upper part of the Cayman Formation on Cayman Brac have $\delta^{13}C_{VPDB}$ values of 1.6 to 3.5‰ (average 2.5‰) and $\delta^{18}O_{VDPB}$ values of 2.3 to 4.0‰ (average 3.2‰), whereas MacNeil and Jones (2003) obtained $\delta^{13}C_{VPDB}$ values of -1.8 to +1.4‰ (average 0.3‰) and $\delta^{18}O_{VDPB}$ values of -0.08 to +2.16‰ (average +1.3‰) from the dolostones from the Pedro Castle Formation. In this study, the isotope values obtained for dolostone from the Cayman Formation beside the Lower Cave yielded values within the range given by Zhao and Jones (2012). Values obtained from a dolomitic limestone from the Pedro Castle Formation bedrock beside the Upper Cave are more negative than those reported by MacNeil and Jones (2003) because it contained ~ 65% calcite (Fig. 24).

O and C isotopes values obtained from the cave deposits can be divided into groups A and B. Group A, which includes the dolostones from the Cayman Formation, the caymanite, and the dolostones in Units A and B in the Upper Cave, are characterized by similar values that are comparable to the values previously reported for the Cayman Formation (Fig. 24). The more negative values for the caymanite in the upper part of the Lower Cave reflects the fact that it contains ~45% calcite cement. Similarly, the more negative values for the dolostones in the lower part of the Upper Cave probably reflects the fact that Units A and B contain ~ 5% and ~ 15% calcite cement, respectively.

Group B includes (1) all of the lithotypes that form the middle and upper parts of the succession in the Upper Cave, and (2) the red and olive terra rossa that fills cavities that crosscut deposits in the Lower Cave and Upper Cave and the bedrock of the Cayman Formation and Pedro Castle Formation (Fig. 24). For these deposits the $\delta^{18}O$ ranges from -4.3 to -6.7‰ and the $\delta^{13}C$ ranges from -6.0 to -11.6‰ (Fig. 24).

4.5. U/Th dating

Dating of two sample of flowstone (Fig. 6E) from the lower part of the Upper Cave indicated that it was more than 500,000 years old.

A speleothem sample from the uppermost part of the Upper Cave (near the Middle Sinkhole) is formed of three parts as defined by colour differences and separation by discontinuities. U/Th dating of each part yielded the following ages (1) >500, 000 years for the basal flowstone layer, (2) 61,953 ± 1,577 years for the basal, incipient stalagmite (4.0 cm in diameter, 0.6 cm high), and (3) 22,303 ± 2,310 years and ~~19261 ± 1,938~~ years for two samples taken from the uppermost part of the stalagmite (4.0 in diameter, 0.7 cm high).

5. Dolomitization

According to Zhao and Jones (2012, their Fig. 12), two phases of dolomitization (I and II), both mediated by seawater, affected the limestones of the Cayman Formation and Pedro Castle Formation. Based on $^{87}Sr/^{86}Sr$ ratios, petrographic evidence, and stratigraphic relationships they offered the following conclusions.

- Phase I occurred in the Late Miocene (6 to 8 Ma) and Phase II occurred during the Pliocene to Early Pleistocene (1 to 5 Ma, but with mode at 2 to 4.5 Ma).
- Phase I dolomitization resulted in partial dolomitization of the Cayman Formation.
- Phase II dolomitization completed dolomitization of the Cayman Formation and dolomitized the lower part of the Pedro Castle Formation.
- Phase II dolomitization took place while sediments of the Pedro Castle Formation were still accumulating.
- Phase II dolomitization was completed before Cayman Brac was tectonically tilted.

6. Geological evolution of lower cave

The notion that the Lower Cave was genetically linked to the Cayman Unconformity that developed during the Messinian lowstand (Jones, 1994; Jones and Hunter, 1994b; Liang and Jones, 2015a) is based on (1) the location of the cave just beneath the unconformity and, (2) at the north end of the cave, there appears to be a short, small-diameter (< 0.5 m) tunnel that connects the cave to the unconformity. The latter suggestion, however, must be treated with some caution because outcrop conditions in that critical area are poor. This architecture is parallel to the situation found in Pedro Castle Quarry on Grand Cayman where a filled cave in the upper part of the Cayman Formation was linked to the Cayman Unconformity (Jones and Smith, 1988, their Fig. 6; Jones, 1992b, his Fig. 2).

The Lower Cave is filled with caymanite, which is not found in the Upper Cave. Although common in the Cayman Formation, caymanite is rare in the Pedro Castle Formation (Jones, 1992a). The original sediments, derived from nearby marine sediments, soils, and swamps were probably transported into caves during severe storms that generated large sea waves that inundated low-lying parts of the island (Jones, 1992a) and/or by surface run-off following heavy rainfall. The presence of marine biofragments attests to the marine influence.

The dolostone that forms the caymanite has stable (O and C) and radiogenic ($^{87}Sr/^{86}Sr$) isotopes similar to those derived from the dolostones of the Cayman Formation (Fig. 24). The $^{87}Sr/^{86}Sr$ ratios from the caymanite are consistent with Phase I dolomitization as defined by Zhao and Jones (2012), which took place 6 to 8 Ma (Late Miocene). These similarities indicate that (1) the original sediments in the cave were deposited before dolomitization took place, and (2) dolomitization of the bedrock and the cavity-filling sediments took place at the same time.

7. Geological evolution of Upper Cave

The Upper Cave is housed in the Pedro Castle Formation except for local areas where the cave floor was cut down into the Cayman Formation (Fig. 4B). The lateral and vertical variability in lithotype distribution in this cave means that it is difficult to produce a single stratigraphic succession that is applicable to all parts of the cave. Nevertheless, a composite section based on available information can be divided into packages I to V (Fig. 24) that reflect the distinct stages involved in the filling of the cave. All of these deposits must be younger than the cave that postdated deposition of the sediments that now form the Pedro Castle Formation.

7.1. Package I (P-I)

This package, 30 cm thick, includes the dolostones of units A and B that contain marine biofragments, including red algae and foraminifera. The marine sediments were transported when the cave was flooded by marine water of when storms washed marine sediment on land and into the cave.

The $^{87}Sr/^{86}Sr$ of these dolostones are similar to those from the dolostones in the Pedro Castle Formation but must young because they are in a cave housed in that formation.

7.2. Package II (P-II)

This package is formed of varicoloured calcareous mudstones (Fig. 6E) that contain scattered foraminifera (Fig. 11C, D). Locally, this unit has a chaotic appearance because many of the mudstone beds were brecciated, probably as a result of desiccation and/or erosion as fast-flowing water moved through the cave. Spaces between the rotated clasts are commonly filled with varicoloured mudstones and various generations of calcite cement (Fig. 6B-D).

The boundary with the underlying dolostones of Unit B is sharp (Fig. 6B), suggesting that deposition of the mudstones postdated dolomitization of units A and B, 1 to 5 Ma. This contrasts with the surrounding bedrock of the Pedro Castle Formation where the boundary between the dolostone and limestone is gradational over a stratigraphic interval of ~ 2 m (MacNeil and Jones, 2003, their Fig. 2).

7.3. Package III (P-III)

Package III is formed largely of red terra rossa that is locally intercalated with yellowish-brown flowstone (Fig. 6E). The terra rossa forms (1) laterally continuous laminae/beds (Fig. 4), (2) terra rossa breccia (Fig. 7A-D), and (3) ooids (Fig. 21). No marine biofragments are present in these deposits. This package, therefore, represents a significant change in character relative to the marine sediments found in the underlying sediment packages. The most obvious source for these sediments is the terra rossa soils found on the surface karst of Cayman Brac, as they are today. The distinctive flowstone, like that found in caves of all ages on the Cayman Islands, formed by precipitation from freshwater that flowed through the cave. U/Th dating of the flowstone indicates that it is more than 500,000 years old.

Although the poor soils of the Cayman Islands were mentioned in earlier studies (e.g., Fawcett, 1888; Billymer, 1946), Ahmad and Jones (1969) were the first to provide some analyses of the soils and Baker (1974) was the first to map the distribution of the different soils on the islands. Both Ahmad and Jones (1969) and Baker (1974) compared the red Cayman soils with the bauxites found on Jamaica. Ahmad and Jones (1969, their Table 1) showed that soils on Grand Cayman were formed largely of chlorite (36%), boehmite (27%), gibbsite (5%), kaolinite (1%), and amorphous Al_2O_3 (5%), SiO_2 (9%), and Fe_2O_3 (15%). They argued that these soils differed from the Jamaican bauxites because they contained more silica but less alumina and iron. Later, Ahmad (1996, his Table 6) provided analyses of other soil samples, including two from Cayman Brac that were formed primarily of gibbsite, boehmite, kaolinite, and smectite along with lesser amounts of mica/illite, quartz, hematite, and goethite. Jones (1992a, his Table 2), using data provided by the Water Authority, Cayman Islands showed that nine samples of terra rossa from the New Hut Farms area on the east end of Grand Cayman contained, on average (based on 9 samples), 20 ppm S, 22 ppm K, 1789 ppm Ca, 418 ppm Mg, 2 ppm Fe, 1 ppm Mn, <1 ppm Zn, < 1 ppm Cu, and 2 ppm Al. The Ca and Mg in these soils probably came from the dolostone bedrock.

The high calcite content in the terra rossa from the Upper Cave is due to the anatomizing arrays of calcite-filled microfractures (Fig. 14). The microfractures may have formed through desiccation of the terra rossa after it had been deposited in the caves. The calcite cements were precipitated from $CaCO_3$ saturated waters that subsequently flowed through the cave.

The origin of the terra rossa breccia is difficult to explain because it is not a clast-supported breccia (Fig. 7A, B). The spaces between the terra rossa clasts are filled with a combination of flowstone and calcareous mudstone (Fig. 7A-D). The flowstone was precipitated from calcite-saturated meteoric waters. Although the source of the calcareous mudstone is unknown because no fossils were found in it, the O and C isotopes indicate that it was strongly influenced by freshwater. The brecciated appearance of the terra rossa may be related to plant root activity. The best developed breccia is found close to the middle sinkhole, which may have once been the site were plants grew in terra rossa, as is commonly seen today on Cayman Brac and Grand Cayman. Evidence of root penetration is apparent at similar depths elsewhere in the cave (Fig. 6A). The presence of roots would explain the separation of the clasts and would have also provided the channels for water flow that led to the precipitation of the flowstone.

The terra rossa ooids in the Upper Cave are similar to those found in the bauxite profiles in the Apennines of South Italy (Mondillo et al., 2011; Boni et al., 2013; Mongelli et al., 2014), Weipa in Australia (Tilley, 1998; Taylor and Eggleton, 2004; Eggleton et al., 2008; Taylor et al., 2008), the Darling Range of Australia (Anand and Paine, 2002; Anand and Verrall, 2011), and northern Saudi Arabia (Al-Mutairi et al., 2015). In many cases, the ooids are documented and illustrated without any comment on how they formed (e.g., Mondillo et al., 2011; Boni et al., 2013; Mongelli et al., 2014). Nadon (1991), however, argued that the Weipa pisoliths developed through glaebularisation or centripetal plasmic accumulation and alteration of preexisting kaolinite via Fe/Al oxihydration prior to formation of the cortices. Taylor and Eggleton (2004) suggested that that the cortices formed around fragments located in a porous weathered substrate and that many cracked as a result of mineral dehydration or desilicification. Although biological processes have generally been ignored, Anand and Verrall (2011) argued that pisoliths in the Darling Range (Australia) formed through the fungal-mediated precipitation of Al and Fe. Features documented for terra rossa ooids from other parts of the world and in the ooids found in the Upper Cave on Cayman Brac include nuclei of variable compositions that appear to be detrital in origin and cortical laminae that vary in appearance from ooid to ooid (Fig. 21). Some of the Cayman ooids are characterized by cortical laminae that are formed of calcite, and/or mixtures of clays and calcite (Fig. 21). The Cayman ooids are held in calcite cement that was probably precipitated after the influx of clays and other terra rossa components had ceased (Fig. 21).

7.4. Package IV (P-IV)

P–IV includes the gastropod coquina (Fig. 7F) and the overlying bed of oncoid limestone (Fig. 23). Although found only in a small, high area of the cave that is located just north of the Middle Sinkhole (Fig. 4B), these facies are significantly different from the underlying facies. The scattered terra rossa lithoclasts (Fig. 7F) and terra rossa ooids (Fig. 23B, D) found in these facies were probably derived from the P-III sediments.

Given the uniformity of shell size and morphology, the gastropods found in the coquina appear to be a single species. Although probably of terrestrial origin, the specific species is unknown. The few shells that remain in the rock are well preserved and show little evidence of transportation. Gastropods and gastropod debris have been recorded from various caves throughout the world including Coco Ree, Jamaica (Goodfriend and Mitterer, 1993), Mé Auré, New Calidonia (Cowie and Grant-Mackie, 2004), and Mugnano Cave, Italy (Iacoviello and Martini, 2012, 2013). In an unnamed cave at Coco Ree, Jamaica, 40 species of land snails (600 to 45,000 yrs B.P.), all endemic to Jamaica, were collected from unconsolidated or poorly cemented bauxitic sediments that overlie similar deposits that have been well-cemented by calcite (Goodfriend and Mitterer, 1993). All of the species found in the cave were also present on the exposed land surfaces around the cave. The setting is similar to that found in the Upper Cave in the West End Quarry on Cayman Brac. Similarly, Cowie and Grant-Makie (2004), documented 20 terrestrial species of gastropods from a cave at Mé Auré in New Caledonia that had accumulated over a time span of ~ 3000 years. In each example, the gastropods appear to have been transported into the cave.

Many oncoids in the bed above the gastropod coquina, have small gastropod shells or fragments of larger shells as their nucleus (Fig. 23). Although the exact conditions under which they formed is difficult to interpret from the limited evidence available, it was probably a high energy setting with water more or less constantly flowing through the area.

7.5. Package V (P-V)

P–V includes the flowstone in the upper part of the cave that lies on top of the terra rossa breccia (P-III), the stalactites and draperies that adorn the cave ceiling close to the Middle Sinkhole (Fig. 7D, E), and rare small stalagmites. These deposits formed from waters that flowed over the cave floor (flowstone) and dripped from the ceiling (stalactites). The calcite cements that filled the microfractures in the underlying terra rossa (Fig. 14), the flowstone that formed around the terra rossa lithoclasts (Fig. 7A-C), and locally on top of the red terra rossa (Fig. 7D) were probably formed from the same waters.

U/Th dating of a flowstone/stalagmite sample from this package yielded ages of >500,000 years (lower flowstone), 64,355 years (lower stalagmite), and 22,500 and 26,353 years old. Such dates attest to the antiquity of the cave and the shows that such precipitation was episodic.

8. Geological evolution of late-stage cavities

Irregular shaped cavities that seem to extend from the present day surface, locally crosscut the bedrock and the deposits in both the Lower Cave and Upper Cave. These cavities are filled with red terra rossa or olive terra rossa. As such, their formation must post-date development of those caves and most of the deposits that fill them. The cavities filled with the olive terra rossa are younger than those filled with the red terra rossa because the former commonly crosscut the latter.

9. Discussion

Well-developed karst terrains with spectacular arrays of caves are common in the carbonate bedrock of many isolated oceanic islands, including those found in the Pacific Ocean (e.g., Rodrigues Island – Burney et al., 2015), the Mediterranean Sea (e.g., Mallorca – Fornós et al., 2009; Fornós et al., 2014), the North Atlantic Ocean (e.g., Bermuda – Palmer et al., 1977; Mylroie, 1984; van Hengstum and Scott, 2012), and the Caribbean Sea (e.g., the Bahamas – Mylroie, 1984; Mylroie et al., 1991). If the caves are partly or completely submerged by seawater they become receptacles for marine sediments (e.g., Fornós et al., 2009; Farrant and Smart, 2011; van Hengstum and Scott, 2012), whereas those in the vadose zone may be characterized by marine sediments, terrestrial sediments, and/or speleothems (e.g., Auler et al., 2009; Farrant and Smart, 2011; van Hengstum et al., 2011; van Hengstum and Scott, 2012). In these dynamic settings, variations in sea level, ~~be they due to eustasy or tectonism~~, will cause a reset of the entire system. Thus, a drop in sea level may place a previously submerged cave in the vadose zone whereas a rise in sea level may lead to submergence of a cave that had been in the vadose zone. Potentially, the deposits found in the caves will provide a record of such changes, which may not be evident from the host bedrock succession. Such is the case for caves developed in the Miocene and Pliocene carbonates on Cayman Brac.

During the late Pliocene and Pleistocene, Cayman Brac was subject to rapid eustatic oscillations in sea level (Fig. 25). Establishing the timing and scale of the eustatic sea level changes is difficult given the contrasting opinions that exist. For example, interpretations of highstand levels during the Mid-Pliocene Warm Period (~3.3 to 2.9 Ma), based on physical features, have yielded estimates of + 35 m from North and South Carolina (Dowsett and Cronin, 1990), +15-20 m from Virginia (Krantz, 1991), +20-25 m from Enewetak Atoll (Wardlaw and Quinn, 1991), +60 m from Alaska (Kaufman and Brighma-Grette, 1993), and +30 m from Roe Plain, Australia (James et al., 2006). This gives an overall range of +15 to 60 m with an average of ~ 34 m. Raymo et al. (2011), however, argued that these estimates were too high because they had not considered all of the factors that have led to the present-day altitudes of the physical features on which these sea levels were based. Their modeling for these areas, which included corrections for (1) local tectonic movements, (2) local sediment loading, (3) changes due to mantle convection flow, and (4) glacial isostatic adjustments reduced the estimated sea-level highstands to +7.9 to 26.8 m (Raymo et al., 2011). Comparison of sea-level curves like those shown in Figure 2A (Miller et al., 2005) and Figure 25B (Hansen et al., 2013), also highlight the contrasts between different models. Thus, caution must be used in assessing the succession on Cayman Brac relative to eustatic sea level variations.

For Cayman Brac, the situation is further complicated because the exact timing of the tectonic tilting to the west is unknown (Zhao and Jones, 2012, 2013; Liang and Jones, 2015a). Two models (I and II) have been invoked to explain the evolution of the bedrock succession, with the key difference being the timing of the tectonic tilting (Zhao and Jones, 2012).

- Model I involves (1) deposition of the Cayman Formation followed by development of the Cayman Unconformity, and later dolomitization, (2) tectonic tilting of the island to the west, and (3) deposition of the Pedro Castle Formation only on the western part of the island.
- Model II involves (1) deposition of the Cayman Formation, (2) development of the Cayman Unconformity, (3) deposition of the Pedro Castle Formation over the entire island, (4)

tectonic tilting of the island, (5) removal, by erosion, of all of the Pedro Castle Formation from the eastern and central parts of the island.

Based on available evidence, Zhao and Jones (2012) adopted Model II and thereby argued that tilting started after the sediments of the Pedro Castle Formation had been deposited. Tilting must have ended prior to deposition of the sediments of the Ironshore Formation, 125,000 years ago, because the associated wave-cut notch (6 m asl) evident in the cliff faces around the island, is horizontal and crosscuts the westward dipping strata of the Cayman Formation and Pedro Castle Formation.

Caves are common on Cayman Brac (Gilleland, 1998), including many with their entrances clearly evident in the cliff faces (Tarhule-Lips and Ford, 1998, 2004). Divided into the "notch caves" (entrances < 2 m above notch) and the "upper caves" (entrances > 2 m above notch), they are characterized by speleothems up to 408,000 years old but little clastic sediment (Tarhule-Lips and Ford, 2004). The notch caves, with some containing speleothems > 200 ka, must have formed before the +6 m notch that developed ~125 ka (Tarhule-Lips and Ford, 2004). Caves located on top of the bluff, inland from the cliff faces, are typically small and decorated with a variety of speleothems (Jones, 2010). Flowstone in the lower part of the Upper Cave in West End Quarry is > 500,000 years old, indicating that some of these caves predated those evident in the cliff faces.

The Lower Cave, housed in the Cayman Formation on Cayman Brac is similar to a filled cave that once existed (now destroyed by blasting) in the Cayman Formation in Pedro Castle Quarry on Grand Cayman that had its floor ~ 9 m below the Cayman Unconformity (Jones and Smith, 1988, their Fig. 6A, B). A tunnel from its west end connected the cave to a large sinkhole that had its opening at the Cayman Unconformity (Jones, 1992b, his Fig. 2). The cave was filled with caymanite, dolomitized wackestone (with marine fossils), red terra rossa, and flowstone (Jones, 1992b, his Fig. 2). Emplacement of the red terra rossa and flowstone postdated the Pedro Castle Formation and dolomitization. The caymanite and marine sediments found in the caves on Cayman Brac and Grand Cayman indicate that both cave entrances must have been open to the influx of the marine sediments. Those sediments must have emplaced prior to deposition of the sediments that now formed the Pedro Castle Formation. As such, both caves had similar developmental histories.

The diverse array of cave-filling sediments and precipitates in the Upper Cave in the West End Quarry on Cayman Brac reflect the complex evolutionary history of that cave. Evident from these deposits (P-I to P-V) are three key evolutionary stages.

- Restriction of dolomitization to P-I. Zhao and Jones (2012) argued that Phase II dolomitization took place while the sediments that now form the Pedro Castle Formation were being deposited. Given that the dolostones of P-I occur in a cave located in the lithified strata of the Pedro Castle Formation, it follows that their dolomitization must have postdated the Phase II dolomitization of Zhao and Jones (2012). The exact age of this late phase dolomitization is, however, impossible to determine because the $^{87}Sr/^{86}Sr$ ratios of the P-I dolostones fall within the range of ratios obtained from the dolostones of the Cayman Formation and Pedro Castle Formation (Fig. 24).
- Transitional conditions of P-II. The lack of dolomite in these mudstones suggests that deposition postdated dolomitization and the presence of foraminifera in the mudstones indicates that the cave was open to marine incursions with its entrance close to sea level. The negative ^{18}O and ^{13}C values of the mudstone, which are lower than those of the

underlying dolostones of P-I, indicate that meteoric waters were involved in their formation.

- With the onset of P-III all connection to the marine environment was lost as shown by the lack of marine sediments in P-III, P-IV, and P-V and the negative ^{18}O and ^{13}C signatures of those deposits (Fig. 24). Package III involve the first precipitation of flowstone and the first influx of terrestrial sediments (Figs. 24, 25) as surface soils (terra rossa) were washed into the cave. U/Th dating indicates that the flowstone in the base of this package is > 500,000 years old, whereas the uppermost speleothems in P-IV are only ~ 21,000 years old.

Development of the notch, upper, and top caves suggests that the core of the island has probably remained above sea level for at least the last 500,000 years and certainly ever since deposition of the sediments that now form the Pedro Castle Formation ended. Since then the uplifted core of the island has been actively eroded. Evidence presented by Liang and Jones (2015a), for example, suggests that as much as 145 m of the Cayman Formation and 45 m of the Pedro Castle Formation have been lost to erosion at East Point, which is ~ 16.3 km to the ENE of the West End Quarry. In the quarry, only the basal 2-3 m of the Pedro Castle Formation remains, meaning that 42-43 m of the formation has been lost to erosion and only the oldest part of the formation remains. Today, the surface of the uplifted core, formed of the Cayman Formation and the Pedro Castle Formation (westernmost part of island only), is characterized by a rugged karst terrain (e.g., Liang and Jones, 2015a, their Fig. 11) with terra rossa accumulations in many of the depressions and sinkholes (e.g., Ahmad, 1996).

The red terra rossa, the most obvious deposit in the Upper Cave (Fig. 4), is significant because it is the first record of terrestrial sediments in the cave. Many of the younger caves on Cayman Brac have "red soils" on their floors that came from the terra rossa soils found on the surface (Tarhule-Lips and Ford, 2004). Although the subject of much debate, Muhs et al. (2007) argued that soils found on limestone islands in the western Atlantic Ocean and Caribbean Sea are formed of (1) insoluble residues derived from the carbonate bedrock, (2) fluvial transport of clays from nearby siliciclastic outcrops, (3) wind-blown dust, and/or (4) volcanic ash. For Cayman Brac, option 2 can be excluded because there are no siliciclastic rocks on the island. Although option 4 is viable, available evidence indicates that volcanic input on Cayman Brac was minimal. The possibility that the soils are formed of insoluble residues is viable given that erosion has removed as much 190 m of limestones/dolostones from parts of Cayman Brac. The limestone and dolostone bedrocks of Cayman Brac, however, are pure and it is doubtful that the loss of 190 m of limestone/dolostone could have produced the volume of soil now found on the island. This notion parallels the conclusions offered by Tracey et al. (1964), Birkeland (1999), and Muhs et al. (1987) for soils found on top of carbonate strata on other islands. It appears, therefore, that most of the soils found on the Cayman Islands were derived largely from wind-borne dust from the Sahara Desert and/or from North America during the last glacial period when winds form the west and northwest transported loess over the Caribbean Sea (Muhs et al., 2007).

Today, the floor of the Upper Cave on Cayman Brac is ~ 5 m asl. Stratigraphic evidence suggests that this cave probably formed over the last 2.0 to 4.5 million years and it must have postdated lithification of the Pedro Castle Formation (Fig. 25). Nevertheless, the precise age for the onset of cave formation is impossible to determine given that the exact age of the uppermost part of the Pedro Castle Formation on Cayman Brac is unknown because erosion has removed everything but the basal part of the formation. Thus, it is impossible to determine if sedimentation was restricted to the lower part of the Pliocene or if it continued throughout the Pliocene.

In the Upper Cave, the base of P-III (~ 5.3 m asl) is significant because it records the time when the cave became isolated from marine influences and was first emplaced in the vadose zone (Fig. 25). That change, however, might have been due to eustatic changes in sea level and/or tectonic uplift of the island. Hansen et al. (2013) suggested that sea levels were +10-20 m throughout most of the Pliocene (Fig. 25B), which would have allowed sediment deposition of the sediments that now form the Pedro Castle Formation but precluded formation of the Upper Cave. This sea level curve also suggests that it was not until the latest Pliocene that sea levels dropped below present day sea level (Fig. 25B). This would have led to exposure of the Pedro Castle Formation and the formation of karst, which would have continued throughout the Pleistocene apart from short-lived highstands (Fig. 25B). If the succession in the Upper Cave is considered relative to this sea level curve, then it could be speculated that the base of P-III is roughly coincident with the Pliocene-Pleistocene boundary. This attractive proposition, however, implicitly assumes that the sea level curve proposed by Hansen et al. (2013) is correct, and ignores the fact that tectonic uplift and tilting was also taking place during this time period.

Tectonic elevation and tilting of the core of Cayman Brac could also have been responsible for emplacement of the Upper Cave into the vadose zone with its entrance beyond the influence of marine waters. Uplift would probably may also have caused fracturing and faulting in the bedrock (cf., Purdy and Waltham, 1999) that, in turn, promoted water circulation and breakdown of the exposed Pedro Castle Formation and Cayman Formation. As uplift proceeded, erosion progressively removed the Pedro Castle Formation and much of the Cayman Formation from the central and eastern parts of the island.

With the information presently available it is impossible to determine if development of the bedrock succession, the caves, and the cave fills was controlled by eustatic sea level changes, tectonic tilting, or some combination of the two. Nevertheless, it is readily apparent that integration of the information derived from the bedrock succession and the cave-filling successions has provided insights into the geological evolution of Cayman Brac that cannot be determined from the bedrock alone.

10. Conclusions

The development of limestone successions on isolated oceanic islands is fundamentally controlled by the interplay between eustatic sea level changes and local tectonic activity. Deposition during the highstands leaves a tangible record of the operative processes, whereas lowstands typically leads to karst formation as dissolution modifies the bedrock. Information on other associated processes, including sediment formation or precipitation, can be difficult to ascertain. This shortcoming, however, can be partly overcome by interpretation of deposits found in caves. This is well illustrated in this study where detailed analysis of cave-filling deposits in the Miocene-Pliocene strata of Cayman Brac has led to the following major conclusions.

- The Lower Cave and the caymanite that fills it developed during the Messinian lowstand. Marine fossils in the caymanite indicate that the cave entrance was open to marine incursions, possibly during storms.
- The Upper Cave is filled with various lithotypes that developed in response to ever changing conditions. The basal sediment packages in this cave formed under marine influences whereas the upper sediment packages were isolated from marine incursions and developed in a meteoric regime.

- U/Th dating indicates that some of the flowstones are > 500,000 years old whereas other flowstone in the uppermost part of the Upper Cave formed ~ 62,000 and 21,000 years ago.
- Late stage cavities that cut across both the Lower Cave and the Upper Cave are filled with red and olive terra rossa with the latter being younger than the former.

Integration of these conclusions with interpretations of the bedrock succession provides valuable information about the subaerial landscape as it evolved while the core of the island remained above sea level.

Acknowledgments

I am grateful to the Natural Sciences and Engineering Research Council of Canada, which funded this research (Grant ZA635 to Jones); Hendrik van Genderen from The Water Authority of Cayman Islands, who provided logistical support and assisted in the field with collection of samples; Mr. M. Scott who granted permission for entry and collection of samples from the West End Quarry on Cayman Brac; Diane Caird who did the XRD analyses; Noga Vaisblat who processed the ion-milling of the terra rossa sample; and Nathan Gerein who operated the SEM used in this study.

FIGURE CAPTIONS

Fig. 1. Location of West End Quarry on Cayman Brac. (A) Location of Cayman Brac in Caribbean Sea. (B) Geological map of Cayman Brac showing location of West End Quarry. Map adapted from Jones (1994). (C) Geological cross-section through Cayman Brac (from X to Y on panel B). Adapted from Jones (1994).

Fig. 2. **(A)** Stratigraphic succession on west end of Cayman Brac. (B) Sea-level curve for last 10 Ma based on data in Miller et al. (2005, Supplemental Table S1 with points plotted every 0.05 Ma interval). Dates for Messinian Salinity Crisis (MSC) onset and termination taken from Jiménez-Moreno et al. (2013). Dates for the periods based on the International Chronostratigraphic Chart (http://www.stratigraphy.org/ICSchart/ChronostratChart2014-02.jpg). Modified from Liang and Jones (2015, their Fig. 2).

Fig. 3. View of northwest corner West End Quarry showing the Cayman Formation (CF), Cayman Unconformity (CUC), Pedro Castle Formation (PCF), and modern karst surface. Note open caves and cavities (C) filled with lithified terra rossa of various colours. Photograph taken in 2006 when quarry floor and top of quarry face were ~ 1.5 m and ~ 8 m above sea level, respectively.

Fig. 4. East wall of West End Quarry showing cross-sections through filled caves. (A) North end of Lower Cave (outlined by black line) in the Cayman Formation (CF), the Cayman Unconformity, the south end of the Upper Cave in the Pedro Castle Formation (PCF), and the "South Sinkhole". (B) Central and north parts of Upper Cave (outlined by black line) and location of "Middle Sinkhole". North end of the cave is not shown because poor outcrop conditions prevents detailed mapping. Red arrow is at same point as red arrow on panel A.

Fig. 5. Lower Cave in the Cayman Formation (Fig. 4A). (A, B) Caymanite with red and off-white laminae defining variable attitudes of the laminae. CF= Cayman Formation. (B, C) Cavities cross-cutting the caymanite and filled with olive terra rossa (OTR) and red terra rossa (RTR).

Fig. 6. Outcrop photographs of deposits in basal part of the Upper Cave housed in the Pedro Castle Formation (Fig. 4A). Panels A-D from south end of cave; panel E from middle part of the cave. CF = Cayman Formation, PCF = Pedro Castle Formation, RTR = red terra rossa, OTR = olive terra rossa, CM = calcareous mudstone; F = flowstone, SC = spar calcite. (A) General view showing base of Upper Cave at the Cayman Unconformity (arrow). Cave fill is divided into units A and B (dolostones), and units C and D (limestone and terra rossa). PD = location of image shown in panel D. (B) Basal parts of Upper Cave showing sharp boundary between the dolostone of Unit B and calcareous mudstones of Unit C. (C, D) Unit C formed of white to red calcareous mudstones and Unit D formed of irregular masses of red terra rossa in a limestone groundmass. Note isolated cavities filled with red and olive terra rossa. (E) Basal part of Upper Cave with flowstone intercalated with red calcareous mudstone and red terra rossa.

Fig. 7. Outcrop photographs of deposits in middle and upper parts of the Upper Cave near the Middle Sinkhole (Fig. 4B). RTR = red terra rossa, S = speleothem, LST = limestone. (A) Terra rossa breccia formed of irregular-shaped masses of red terra rossa held in groundmass formed of speleothemic calcite and limestone. Note open cavities. (B) Enlarged view from lower right part of panel A showing showing spaces between the masses of red terra rossa filled with speleothemic calcite and limestone. (C) Enlarged view showing red terra rossa coated with thinly laminated speleothemic calcite and central cavity filled with limestone.

(D) Upper part of cave filled with terra rossa breccia overlain by speleothemic calcite and stalactites and draperies hanging from cave roof. PE indicates drapery shown in panel E. (E) Ornate drapery hanging from cave roof. (F) Uppermost part of cave fill formed of gastropod shells embedded in matrix formed of coated grains held in spar calcite cement.

Fig. 8. Thin section photomicrographs of caymanite (all dolomite) from Lower Cave. (A) Laminae defined by subtle variations in colour and grain sizes. (B) Grainstone laminae overlying mudstone laminae. (C) Small red algae biofragments in grainstone laminae. (D) Planktonic foraminifera in mudstone laminae.

Fig. 9. SEM photomicrographs of caymanite from Lower Cave. (A) Finely crystalline dolomite groundmass with small pores lined with limpid dolomite (LD). (B) Caymanite from upper part of cave, formed of very finely crystalline dolomite (left side) with pore lined by limpid dolomite (LD) and filled with calcite (C).

Fig. 10. SEM photomicrographs of finely crystalline dolostones from units A (A-C) and B (D-F) in Upper Cave (Fig. 6A). (A) Finely crystalline dolostone with pore filled with calcite (C). (B) Enlarged view of dolostone showing interlocking dolomite crystals. (C) Dolomitized red algae fragment held in dolostone matrix. (D) Finely crystalline dolostone from Unit B. (E) Enlarged view of dolostone showing interlocking euhedral dolomite crystals. (F) Hollow dolomite crystals, Unit B.

Fig. 11. Thin section photomicrographs of calcareous mudstones from Unit C in Upper Cave (Fig. 6A). Images A-D, unstained thin section; E-G stained with Alizarin Red S Solution. (A) White mudstone with microfractures and cavities lined with calcite cement. (B) Graded bedding in dipping pink mudstone laminae. (C, D) Examples of foraminifera in calcareous mudstones. (E) Microbrecciated calcareous mudstone with calcite cement. (F) Small cavity

with small clasts at base, each surrounded by calcite cement, overlain by mudstone that is coated with calcite cement. (G) Fracture through mudstone lined with calcite cement and filled with olive terra rossa.

Fig. 12. SEM photomicrographs of calcareous mudstones from Unit C. (A, B) General and enlarged views of white mudstone. (C) Red mudstone with small cavity filled with spar calcite cement. (D) Red mudstone with disseminated patches of Fe-rich precipitates (arrows). (E) Enlarged view of Fe-rich mass covered with interlocking plate-shaped crystals. Point A – EDS analysis (see Fig. 13 A). (F) Enlarged view of plate-shaped crystals from panel E. Area B – EDS analysis (see Fig. 13B). (G) Rounded mass of Fe-rich precipitate, from off-white mudstone, formed of trigonal-shaped subcrysals. Point C – EDS analysis (see Fig. 13C). (H) Series of linked Fe-rich precipitates in off-white calcareous mudstone. I indicates position of image shown in panel I. (I) Enlarged view of Fe-precipitate. Point D – EDS analysis (see Fig. 13D). (J) Two ovate masses of Fe-precipitates, each formed of rounded subcrystals. Point E – EDS analysis (see Fig. 13E). (K) Agglomeration of small Fe-rich precipitates in white mudstone. L indicates position of image shown in panel L. (L) Fe-rich precipitate formed of rounded subcrystals. Point F – EDS analysis (see Fig. 13F).

Fig. 13. EDS analyses for Fe-rich precipitates found in calcareous mudstones shown in Figure 12. Weight percentages of elements determined from EDS analyses.

Fig. 14. Thin section and BSE images of red terra rossa. (A-C) Thin section photomicrographs of terra rossa (yellow to orange) dissected by anatomizing arrays of calcite-filled microfractures. (D, E) BSE images of polished surface showing contrast between red terra rossa (dark grey) and calcite-filled fractures (light grey). (F) Elemental map of surface shown in panel E (Ca and Al are in same positions on both panels) showing distribution of Al

(yellow) relative to calcite (red). Al-rich areas also contain Si and Fe. (G) Thin section photomicrograph showing bands of yellowish calcite between bands of red terra rossa. (H) BSE image of same area as in panel G, showing contrast between the calcite (light grey) and red terra rossa (dark grey). Line X-Y indicates position of line transect shown in Figure 15. (I) Enlarged view from lower part of panel G showing alternating bands of fibrous calcite and red terra rossa.

Fig. 15. Compositional transect along line X-Y (Fig. 14H), showing contrast between the calcite and red terra rossa. Minor elements, not shown in this diagram are Ti, Mg, and K (~ 4 wt% in total), are found largely in the red terra rossa. Based on 100 equally-spaced points of analysis.

Fig. 16. SEM photomicrographs of micro-milled surface of red terra rossa. Elemental content based on EDS analyses. (A-C) Groundmass of lath-shaped crystals (Al and Si) of two size-classes with disseminated Fe-oxide grains (Fe). (D) Mass of Fe-oxide in terra rossa matrix. (E) Disseminated Fe-oxide grains in terra rossa matrix. (F) Euhedral zircon crystal (Zr and Si). (G) Ti-rich grain. (H) Grain formed of Cr and Fe. (I) Grain formed of P, Ce, and La.

Fig. 17. Thin section photomicrograph (A) and BSE images (B-E) of terra rossa in terra rossa breccia. (A) Contrasting colours of terra rossa evident in thin section. (B) BSE image of central part of panel A (white arrow indicates common point) showing calcite-filled (Ca) fractures and lack of contrast between the different coloured terra rossa. (C) Enlarged view from panel B (white arrow indicates common point) showing lack of contrast between different coloured terra rossa and location of transect shown in Figure 18. D and E indicate location of areas shown in panels D and E. (D, E) Comparison of disseminated Fe (white) in different coloured terra rossa.

Fig. 18. EDS analyses along transect U-V (Fig. 17C). For ease of comparison, the weight % of Al, Si, Fe, and Ti have been added together (ASFT) given that they are always associated with each other in the terra rossa. Based on 100 equally spaced points of analysis.

Fig. 19. Thin section photomicrographs (A, B, D) and BSE images (C, E) of olive terra rossa. (A) Variations in colour of olive terra rossa as seen in plane polarized light. Letters B and D indicate locations of panels B and D, respectively. (B) Enlarged view of bright red area of terra rossa (panel A) showing subtle colour variations. (C) BSE image of same area as panel B and location of transect W-X (Fig. 20A). (D) Enlarged view of terra rossa (panel A) with array of calcite-filled microfractures. (E) BSE image of same area shown in panel D and location of transect Y-Z (Fig. 20B). Calcite-filled microfractures highlighted by light grey colour.

Fig. 20. EDS line transects along lines W-X (Fig. 19C) and Y-Z (Fig. 19E). Each transect is based on 100 equally spaced points of analysis. Note difference in Ca levels between the two transects.

Fig. 21. Paired thin section photomicrographs (top) and BSE images (bottom) showing variations in structures and composition of terra rossa ooids from Unit D (Fig. 6C). Black-white-yellow lines on BSE images show EDS transects for compositional analyses shown in Figure 22. Black = line of transect; white = nucleus of ooid; yellow = cortical laminae and correspond to zones indicated on transects in Figure 22. Ooids held in calcite groundmass.

Fig. 22. EDS analyses showing contrast in distribution of calcium (C) and Al+Si+Fe+Ti (ASFT) of terra rossa ooids shown in Figure 21. Dashed lines indicate boundaries between the nuclei (N) and cortical laminae (C) of ooids as indicate in Figure 22. Each transect is based on 100 equally spaced points of analysis.

Fig. 23. Thin section photomicrographs of coated grains from uppermost part of Upper Cave near the Middle Sinkhole. All images with plane polarized light. Blue = porosity. (A, B) Gastropod shells coated with thin micrite laminae and isopachous calcite rim. Interiors partly filled with terra rossa ooids and calcite cement. (C) Group of small coated grains, each with shell fragment as its nucleus. (D) Enlarged view of uppermost coated grain from panel C showing nucleus formed of shell fragment and successive layers of micrite highlighted by subtle differences in colour. (E) Group of coated grains with nuclei formed of shell fragments and encased by isopachous calcite cement. Note small terra rossa ooids between the coated grains. (F) Coated grain formed large micrite nucleus encased by micrite layers.

Fig. 24. Schematic stratigraphic column (not to scale) showing (A) bedrock succession, the Lower Cave, and cave deposits in the Upper Cave that are divided into genetically related packages P-I to P-V. (B) ^{18}O and ^{13}C isotopes for different lithotypes found in the caves (circles) relative to the ranges of values (bars) for the Cayman Formation (Zhao and Jones, 2012) and Pedro Castle Formation (from MacNeil and Jones, 2003). (C) ^{87}Sr/^{86}Sr ratios for the dolostones in the lower and Upper Caves (squares) relative to the ^{87}Sr/^{86}Sr ratios for the dolostones (bars) in the Cayman Formation and Pedro Castle Formation (MacNeil and Jones, 2003; Zhao and Jones, 2012).

Fig. 25. Integration of paragenetic stages in evolution of bedrock succession (A) and cave-fill succession (C) relative to sea-level changes over the last 5.33 myrs (from Hansen et al., 2013, their Fig. 2b). Pliocene-Pleistocene boundary is placed at 2.58 myrs rather than at 1.8 myrs as shown by Hansen et al. (2013).

REFERENCES

Ahmad, N., 1996. Agricultural land capability of the Cayman Islands.

Ahmad, N., Jones, R.L., 1969. Occurrence of aluminous lateritic soils (bauxites) in the Bahamas and Cayman Islands. Economic Geology 64, 804-808.

Al-Mutairi, A.N., Galmed, M.A., Aldamegh, K.S., 2015. Petrogenesis of the Az Zabirah south zone bauxite ore deposits, central northern Saudi Arabia. Arabian Journal of Geoscience 8, 2327-2339.

Alonso-Zarza, A.M., Wright, V.P., 2010. Calcretes. In: A.M. Alonso-Zarza and L.H. Tanner (Eds.), Carbonates in Continental Settings. Facies, Environments and Processes. Developments in Sedimentology. Elsevier, Amsterdam, The Netherlands, pp. 225-267.

Anand, R.R., Paine, M., 2002. Regolith geology of the Yilgarn Craton, Westrn Australia: implications for exploration. Australian Journal of Earth Sciences 49, 4-162.

Anand, R.R., Verrall, M., 2011. Biological origin of minerals in pisoliths in the Darling Range of Western Australia. Australian Journal of Earth Sciences 58, 823-833.

Auler, A.S., Smart, P.L., Wang, X., Piló, L.B., Edwards, R.L., Cheng, H., 2009. Cyclic sedimentation in Brazilian caves: Mechanisms and palaeoenvironmental significance. Geomorphology 106, 142-153.

Baker, R.J., 1974. Soil and land-use survey No. 26 Cayman Islands, The Regional Research Centre, Department of Soil Science, University of the West Indies.

Billymer, J.H.S., 1946. The Cayman Islands. Geographical Review 36, 29-43.

Birkeland, P.W., 1999. Soils and Geomorphology. Oxford University Press, New York.

Boni, M.R., G., Mondillo, N., Balassone, Santoro, L., 2013. Quantitative mineralogical charaterization of karst bauxite deposits in the Southern Apennines, Italy. Economic Geology 108, 813-833.

Burney, D.A., Hume, J.P., Middleton, G.J., Steel, L., Burney, L.P., Porch, N., 2015. Stratigraphy and chronology of karst featurs on Rodrigues Island, southwestern Indian Ocean. Journal of Cave and Karst Studies 77, 37-51.

Choquette, P.W., James, N.P., 1998. Introduction. In: N.P. James and P.W. Choquette (Eds.), Paleokarst. Springer-Verlag, Berlin, Gernany, pp. 1-21.

Clari, P.A., Pierre, F.D., Martire, L., 1995. Discontinuities in carbonate successions: Identification, interpretation and classification of some Italian examples. Sedimentary Geology 100, 97-121.

Cowie, R.H., Grant-Mackie, J.A., 2004. Land snail fauna of Mé Auré Cave (WMD007), Moindou, New Caledonia: Human introductions and faunal change. Pacific Science 58, 447-460.

Dowsett, H.J., Cronin, T.M., 1990. High eustatic sea level during the middle Pliocene: Evidence from the southeastern U.S. Atlantic Coastal Plain. Geology 18(5), 435-438.

Durn, G., Ottner, F., Slovenec, D., 1999. Mineralogical and geochemical indicators of the polygenetic nature of terra rossa in Istria, Crotia. Geoderma 91, 125-150.

Eggleton, R.A., Taylor, G., Le Gleuher, M., Foster, L.D., Tilley, D.B., Morgan, C.M., 2008. Regolith profile, mineralogy and geochemistry of the Weipa bauxite, northern Australia. Australian Journal of Earth Sciences 55, S17-S43.

Esteban, M., Klappa, C.F., 1983. Subaerial exposure environment In: P.A. Scholle, D.G. Bebout and C.H. Moore (Eds.), Carbonate Depositional Environments. American Association of Petroleum Geologists, Tulsa, United States, pp. 1-54.

Farrant, A.R., Smart, P.L., 2011. Role of sediment in speleogenesis: Sedimentation and paragenesis. Geomorphology 134, 79-93.

Fawcett, W., 1888. Cayman Islands. Bulletin of Miscellaneous Information (Royal Botanic Gardens, Kew) 1888, 160-163.

Folk, R.L., Land, L.S., 1975. Mg/Ca ratio and salinity: Two controls over crystallization of dolomite. American Association of Petroleum Geologists Bulletin 59, 60-68.

Folk, R.L., McBride, E.F., 1976. The Caballos Novaculite revisited - Part 1: Origin of novaculite members. Journal of Sedimentary Petrology 46, 659-669.

Folk, R.L., Siedlecka, A., 1974. The schizohaline environment: Its sedimentary and diagenetic fabrics as exemplified by Late Paleozoic rocks of Bear Island, Svalbard. Sedimentary Geology 11, 1-15.

Foos, A.M., Sasawsky, I.D., LaRock, E.J., Kambesis, P.N., 2000. Detrital origin of a sedimentary fill, Lechuguilla Cave, Guadalupe Mountains, New Mexico. Clays and Clay Minerals 48, 693-698.

Fornós, J.J., Ginés, F., Gràcia, F., Merino, A., Gómez-Pujol, L., Bover, P., 2014. Cave deposits and sedimentary processes in Cova des Pas de Vallgornera (Mallorca, Western Mediterranean). International Journal of Speleology 43, 159-174.

Fornós, J.J., Ginés, J., Ginés, F., 2009. Present-day sedimentary facies in the coastal karst caves on Mallorca Island (Western Mediterranean). Journal of Cave and Karst Studies 71, 86-99.

Gilleland, T., 1998. The caves of Cayman Brac. National Speleological Society News, 202-207.

Ginés, A., Ginés, J., 2007. Eogenetic karst, glaioeustatic cave pools and anchialine enviroments on Mallorca Island: a discussion of coastal speleogenesis. International Journal of Speleology 36, 57-67.

Ginés, J., Ginés, A., Pomar, L., 1981. Morphological and mineralogical features of phreatic spelothems occurring in coastal caves of Majorca (Spain). 2, 529-532.

Goodfriend, G.A., Mitterer, R.M., 1993. A 45,000-yr record of a tropical lowland biota: The land snail fauna from cave sediments at Coco Ree, Jamaica. Geological Society of America Bulletin 105, 18-29.

Hansen, J.K., Sato, M., Russell, G., Kharecha, P., 2013. Climate sensitivity, sea level and atmospheric carbon dioxide. Philosophical Transactions of the Royal Society A 371.

Hillgartner, H., 1998. Discontinuity surfaces on a shallow-marine carbonate platform (Berriasian, Valaginian, France and Switzerland). Journal of Sedimentary Petrology 68, 1093-1108.

Iacoviello, F., Martini, I., 2012. Provenance and geological significance of red mud and other clastic sediments of the Mugnano Cave (Montagnola Senese, Italy). International Journal of Speleology 41, 317-328.

Iacoviello, F., Martini, I., 2013. Clay minerals in cave sediments and terra rossa soils in the Montagnola Senese karst massif (Italy). Geological Quarterly 57, 527-536.

James, N.P., Bone, Y., Carter, R.M., Murray-Wallace, C.V., 2006. Origin of the Late Neogene Roe Plains and their calcarenite veneer: Implications for sedimentology and tectonics in the Great Australian Bight. Australian Journal of Earth Sciences 53, 407-419.

Jiménez-Moreno, G., Pérez-Asensio, J.N., Larrasoaña, J.C., Aguirre, J., Civis, J., Rivas-Carballo, M.R., Valle-Hernández, M.F., González-Delgado, J.A., 2013. Vegetation, sea-level and climate changes during the Messinian salinity crisis Geological Society of America 125, 432-444.

Jones, B., 1992a. Caymanite, a cavity-filling deposit in the Oligocene-Miocene Bluff Formation of the Cayman Islands. Canadian Journal of Earth Sciences 29, 720-736.

Jones, B., 1992b. Void-filling deposits in karst terrains of isolated oceanic islands: A case study from Tertiary carbonates of the Cayman Islands. Sedimentology 39, 857-876.

Jones, B., 1994. Geology of the Cayman Islands. In: M.A. Brunt and J.E. Davies (Eds.), The Cayman Islands: Natural History and Biogeography. Kluwer, Dordrecht, The Netherlands, pp. 13-49.

Jones, B., 2010. The preferential association of dolomite with microbes in stalactites from Cayman Brac, British West Indies. Sedimentary Geology 226, 94-109.

Jones, B., Hunter, I.G., 1994a. Evolution of an isolated carbonate bank during Oligocene, Miocene, and Pliocene times, Cayman Brac, British West Indies. Facies 30, 25-50.

Jones, B., Hunter, I.G., 1994b. Messinian (Late Miocene) karst on Grand Cayman, British West Indies: An example of an erosional sequence boundary. Journal of Sedimentary Research 64, 531-541.

Jones, B., Luth, R.W., MacNeil, A.J., 2001. Powder X-ray analysis of homogeneous and heterogeneous dolostones. Journal of Sedimentary Research 71, 791-800.

Jones, B., Smith, D.S., 1988. Open and filled karst features on the Cayman Islands: Implications for the recognition of paleokarst. Canadian Journal of Earth Sciences 25, 1277-1291.

Kaldi, J., Gidman, J., 1982. Early diagenetic dolomite cements: Examples from the Permian Lower Magnesian Limestone of England and the Pleistocene carbonates of the Bahamas. Journal of Sedimentary Petrology 52, 1073-1085.

Kaufman, D.S., Brighma-Grette, J., 1993. Aminostratigraphic correlations and paleotemperatue implicaitons, Plioce-Pleistocene high-sea-level deposits =, northwestern Alaska. Quaternary Science Reviews 12, 21-33.

Krantz, D.E., 1991. A chronology of Pliocene sea-level fluctuations: the U.S. middle Atlantic plain record. Quaternary Science Reviews 10, 163-174.

Liang, T., Jones, B., 2014. Deciphering the impact of sea-level changes and tectonic movement on erosional sequence boundaries in carbonate successions: A case study from Tertiary strata on Grand Cayman and Cayman Brac, British West Indies. Sedimentary Geology 305 17-34.

Liang, T., Jones, B., 2015a. Ongoing, long-term evolution of an unconformity that originated as a karstic surface in the Late Miocene: A case study from the Cayman Islands, British West Indies. Sedimentary Geology 322, 1-18.

Liang, T., Jones, B., 2015b. Petrographic and geochemical features of sinkhole-filling deposits associated with an erosional unconformity on Grand Cayman. Sedimentary Geology 315, 64-82.

Lockhart, E.B., 1986. Nature and genesis of caymanite in the Oligocene-Miocene Bluff Formation of Grand Cayman, British West Indies, University of Alberta, Edmonton.

Longman, M.W., Mench, P.A., 1978. Diagenesis of Cretaceous limestone in the Edwards aquifer system of south-central Texas: A scanning electron microscope study. Sedimentary Geology 21, 241-276.

Ludwig, K.R., Paces, J.B., 2002. Uranium-series dating of pedogenic silica and carbonate, Crater Flat, Nevada. Geochimica et Cosmochimica Acta 66, 487-506.

MacNeil, A.J., Jones, B., 2003. Dolomitization of the Pedro Castle Formation (Pliocene), Cayman Brac, British West Indies. Sedimentary Geology 162, 219-238.

Martini, I., 2011. Cave clastic sediments and implications for speleogenesis: New insights form the Mugnano Cave (Montagnola Senese, Northern Apennines, Italy). Geomorphology 134, 452-460.

Merino, E., Banerjee, A., 2008. Terra rossa genesis, implications for karst, and eolian dust: A genetic thread. Journal of Geology 116, 62-75.

Miller, K.G., Kominz, M.A., Browning, J.V., Wright, J.D., Mountain, G.S., Katz, M.E., Sugarman, P.J., Cramer, B.S., Christie-Blick, N., Pekar, S.F., 2005. The Phanerozoic record of global sea-level change. Science 310, 1293-1298.

Mondillo, N., Balassone, G., Boni, M., Rollinson, G., 2011. Karst bauxites in the Campania Apennines (southern Italy): A new approach. Periodico di Mineralogia 80, 407-432.

Mongelli, G., Boni, M., Buccione, R., Sinisi, R., 2014. Geochemistry of the Apulian karst bauxites (southern Italy): Chemical fractionation and parental affinities. Ore Geology Reviews 63, 9-21.

Muhs, D.R., Budahn, J.R., Prospero, J.M., Carey, S.N., 2007. Geochemical evidence for African dust inputs to soils of western Atlantic islands: Barbados, the Bahamas, and Florida. Journal of Geophysical Research 112, 1-26.

Muhs, D.R., Crittenden, R.C., Rosholt, J.N., Bush, C.A., Stewart, K.G., 1987. Genesis of marine terrace soils, Barbados, West Indies: Evidence from mineralogy and geochemistry. Earth Surface Processes and Landforms 12, 605-618.

Mylroie, J.E., 1984. Speleogenetic contrast between the Bermuda and Bahamas Islands, Proceedings of the 2nd Symposium on the Geology of the Bahamas, pp. 113-128.

Mylroie, J.E., Carew, J.L., 1995. Karst development on carbonate islands. In: D.A. Budd, A.H. Saller and P.A. Harris (Eds.), Unconformities in Carbonate Strata – Thier Recognition and the Significance of Associated Porosity. American Association of Petroleum Geologists Memoir, pp. 55-73.

Mylroie, J.E., Carew, J.L., Sealey, N.E., Mylroie, J.R., 1991. Cave development on New Providence Island and Long Island, Bahamas. Cave Science 18, 139-151.

Nadon, D.B., 1991. Introduction to the Petrology of Soils and Chemical Weathering. Wiley, New York, 313 pp.

Palmer, A.N., Palmer, M.V., Queen, T.M., 1977. Geology and origin of the caves of Bermuda. In: T.D. Ford (Ed.), Proceedings of the 7th International Speleological Congress, Sheffield. British Cave Research Association, Bridgewater, U. K., pp. 336-338.

Purdy, E.G., Waltham, D., 1999. Reservoir implication of modern karst topography. American Association of Petroleum Geologists Bulletin 83, 1774-1794.

Raymo, M.E., Mitrovica, J.X., O'Leary, M.J., DeConto, R.M., Hearty, P.J., 2011. Departures from eustasy in Pliocene sea-level records. Nature Geoscience 4, 328-332.

Rigby, J.K., Roberts, H.H., 1976. Geology, reefs and marine communities of Grand Cayman Island, B.W.I., 4. Brigham Young University, Geology Studies, Special Publication no. 4, 97 pp.

Sattler, U., Immenhauser, A., Hillgärtner, H., Esteban, M., 2005. Characterization, lateral variation and lateral extent of discontinuity surfaces on a carbonate platform (Barremian to Lower Aptian, Oman). Sedimentology 52, 339-361.

Smart, P.L., Palmer, R.J., Whitaker, F., Wright, V.P., 1988. Neptunian dikes and fissue fills: An overview and account of some modern examples. In: N.P. James and P.W. Choquette (Eds.), Paleokarst. Springer-Verlag Ltd., New York, pp. 149-163.

Tarhule-Lips, R.F.A., Ford, D.C., 1998. Condensation corrosion in caves on Cayman Brac and Isla de Mona. Journal of Cave and Karst Studies 60, 84-95.

Tarhule-Lips, R.F.A., Ford, D.C., 2004. Karst on Cayman Brac. Zeitschrift für Geomorphologie Supplementband 136, 69-88.

Taylor, G., Eggleton, R.A., Foster, L.D., Tilley, D.B., Le Gleuher, M., Morgan, C.M., 2008. Nature of the Weipa bauxite deposite, northern Australia. Australian Journal of Earth Sciences 55, S45-S70.

Taylor, G., Eggleton, T., 2004. "Little Balls" The origin of the Weipa bauxite. Regolith, 350-354.

Tilley, D.B., 1998. The evolution of bauxite pisoliths at Weipa in northern Queensland. Geological Society of Australia Special Publication 20, 148-156.

Tracey, J.I., Schlanger, S.O., Stark, J.T., Doan, D.B., May, H.G., 1964. General geology of Guam. U.S. Geological Survey, Professional Paper 403-A, 104.

Tućan, F., 1912. Terra rossa, deren natur and entschung. Jahrbuch für Mineralogie, Geologie und Palaontologie 34, 401-430.

van Hengstum, P.J., Scott, D.B., 2012. Sea-level rise and coastal circulation controlled Holocene groundwater development in Bermuda and caused a meteoric lens to collapse 1600 years ago. Marine Micropaleontology 90-91, 29-43.

van Hengstum, P.J., Scott, D.B., Gröcke, D.R., Charette, M.A., 2011. Sea level controls sedimentation and environments in coastal caves and sinkholes. Marine Geology 286, 35-50.

Wardlaw, B.R., Quinn, T.M., 1991. The record of Pliocene sea-level change at Enewetok Atoll. Quaternary Science Reviews 10, 163-174.

Zhao, H., Jones, B., 2012. Origin of "island dolostones": A case study from the Cayman Formation (Miocene), Cayman Brac, British West Indies. Sedimentary Geology 243-244, 191-206.

Zhao, H., Jones, B., 2013. Distribution and interpretation of rare earth elements and yttrium in Cenozoic dolostones and limestones on Cayman Brac, British West Indies. Sedimentary Geology 284-285, 26-38.

Figure 1
Click here to download high resolution image

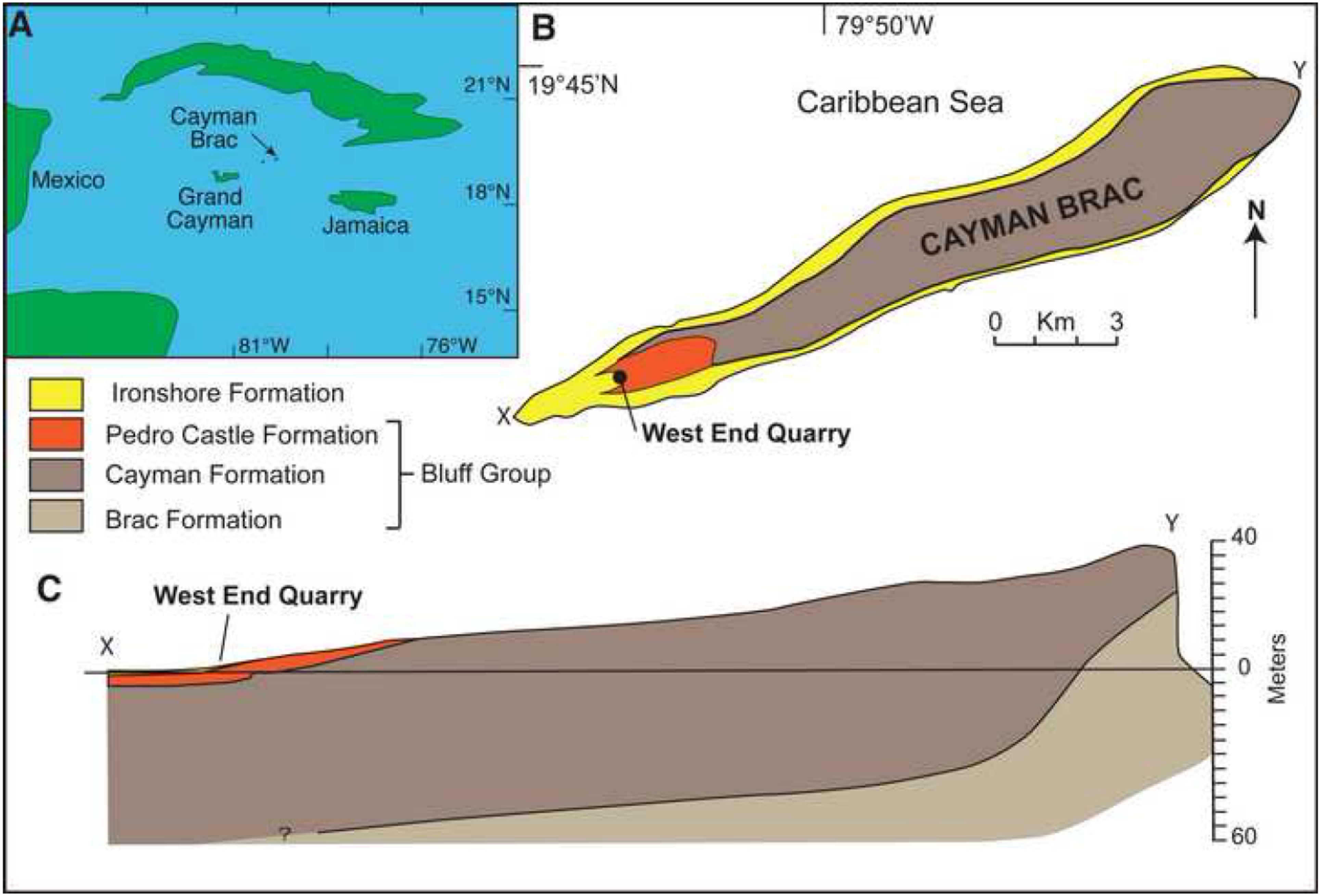

Figure 2
Click here to download high resolution image

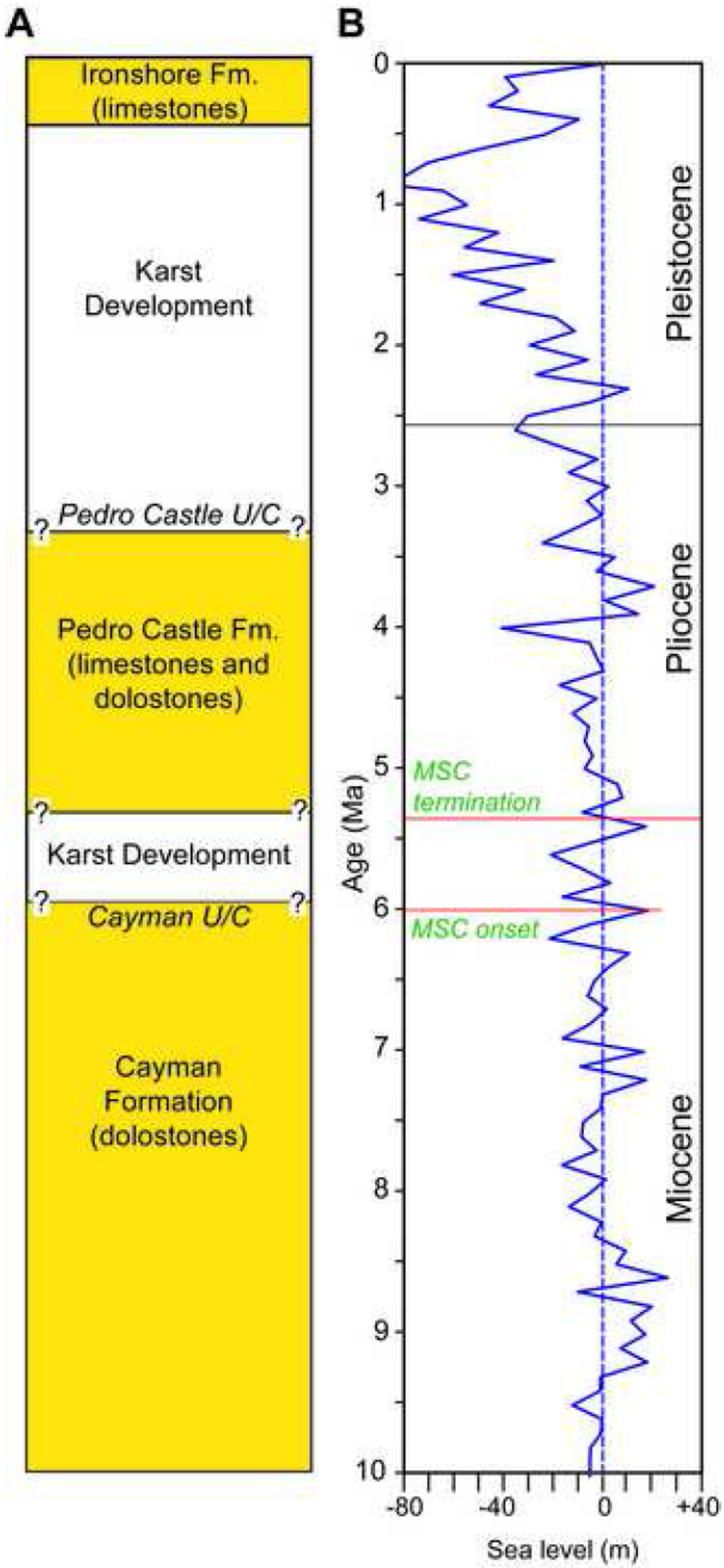

Figure 3
Click here to download high resolution image

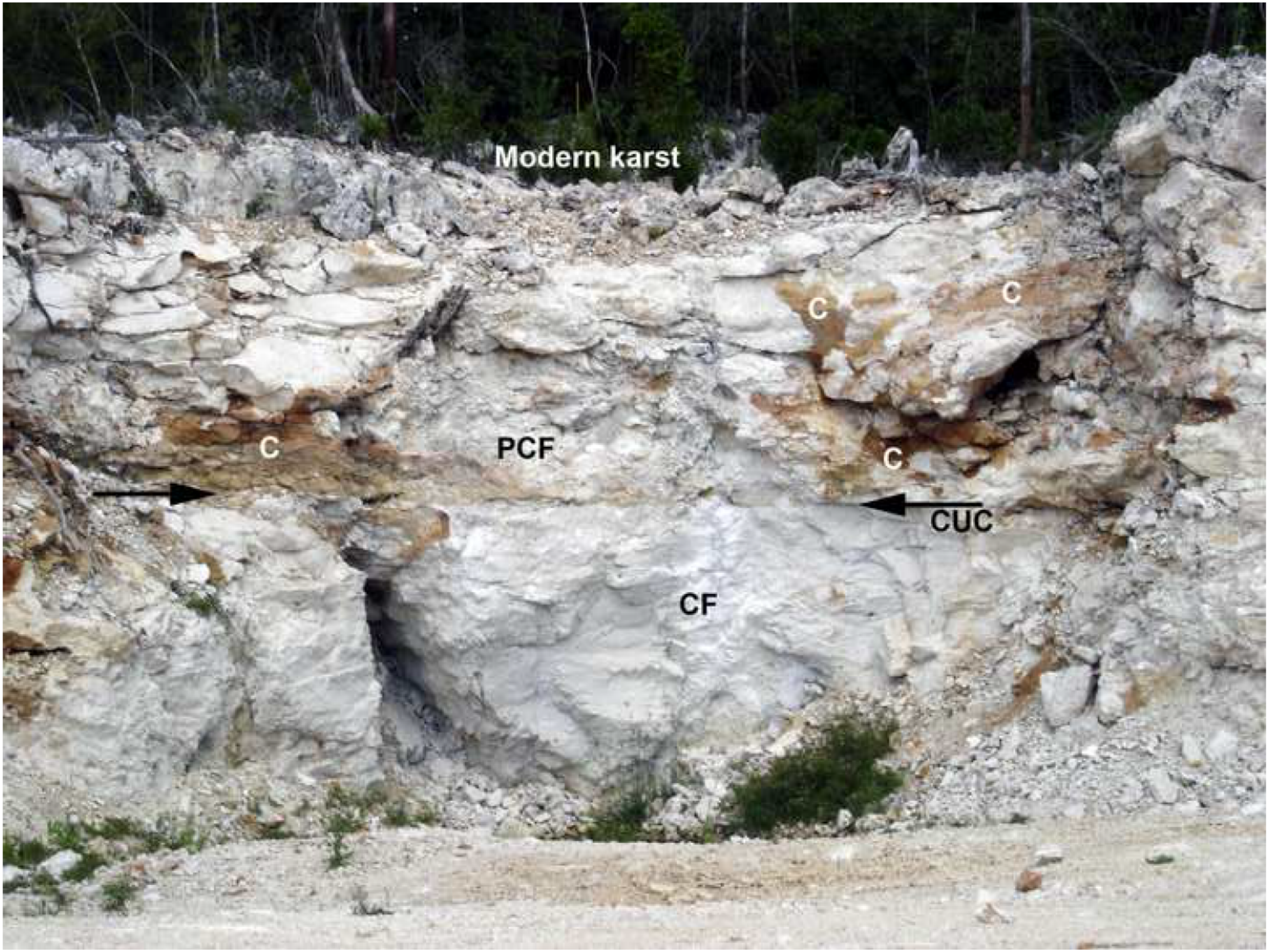

Figure 4
Click here to download high resolution image

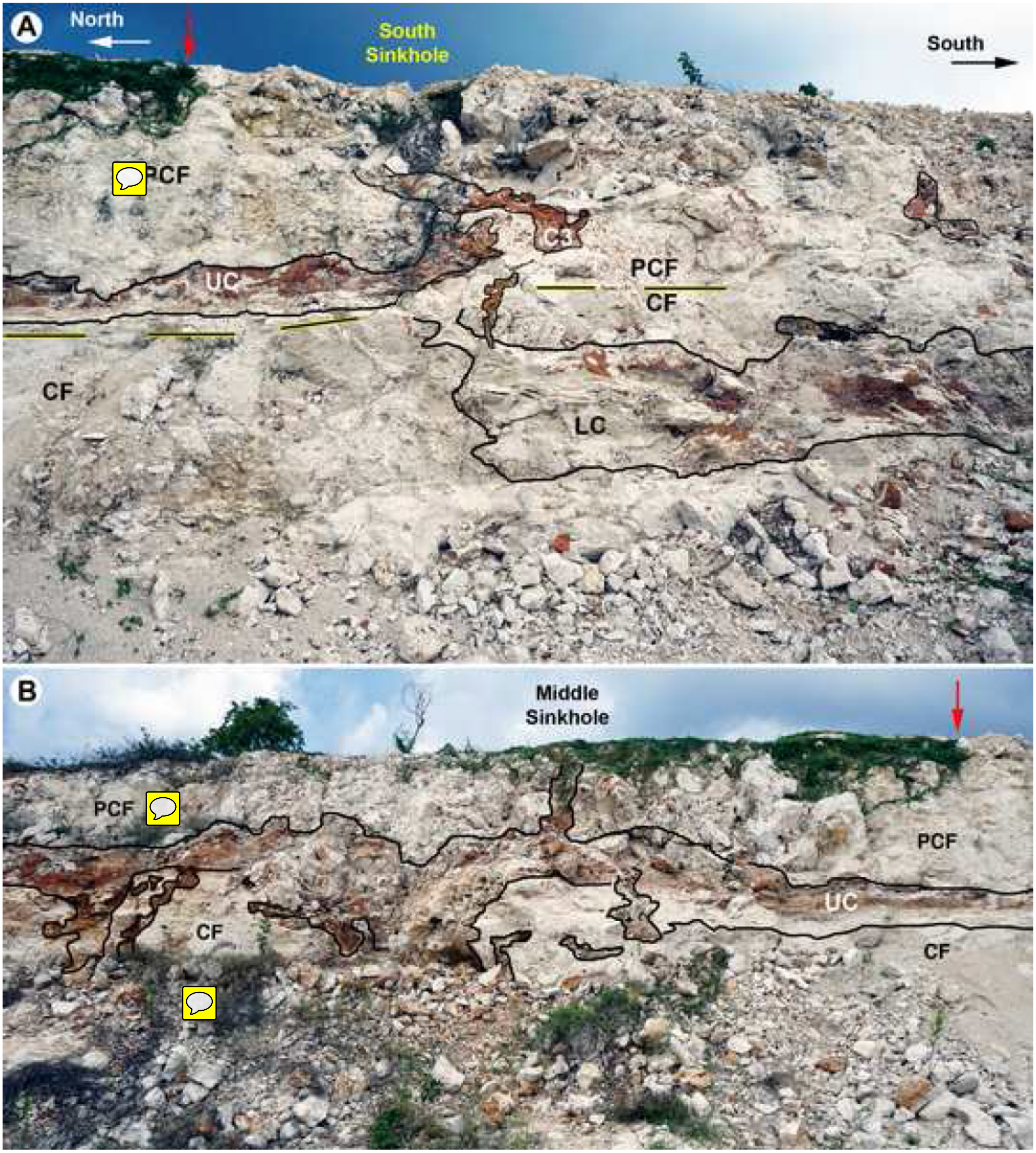

Figure 5
Click here to download high resolution image

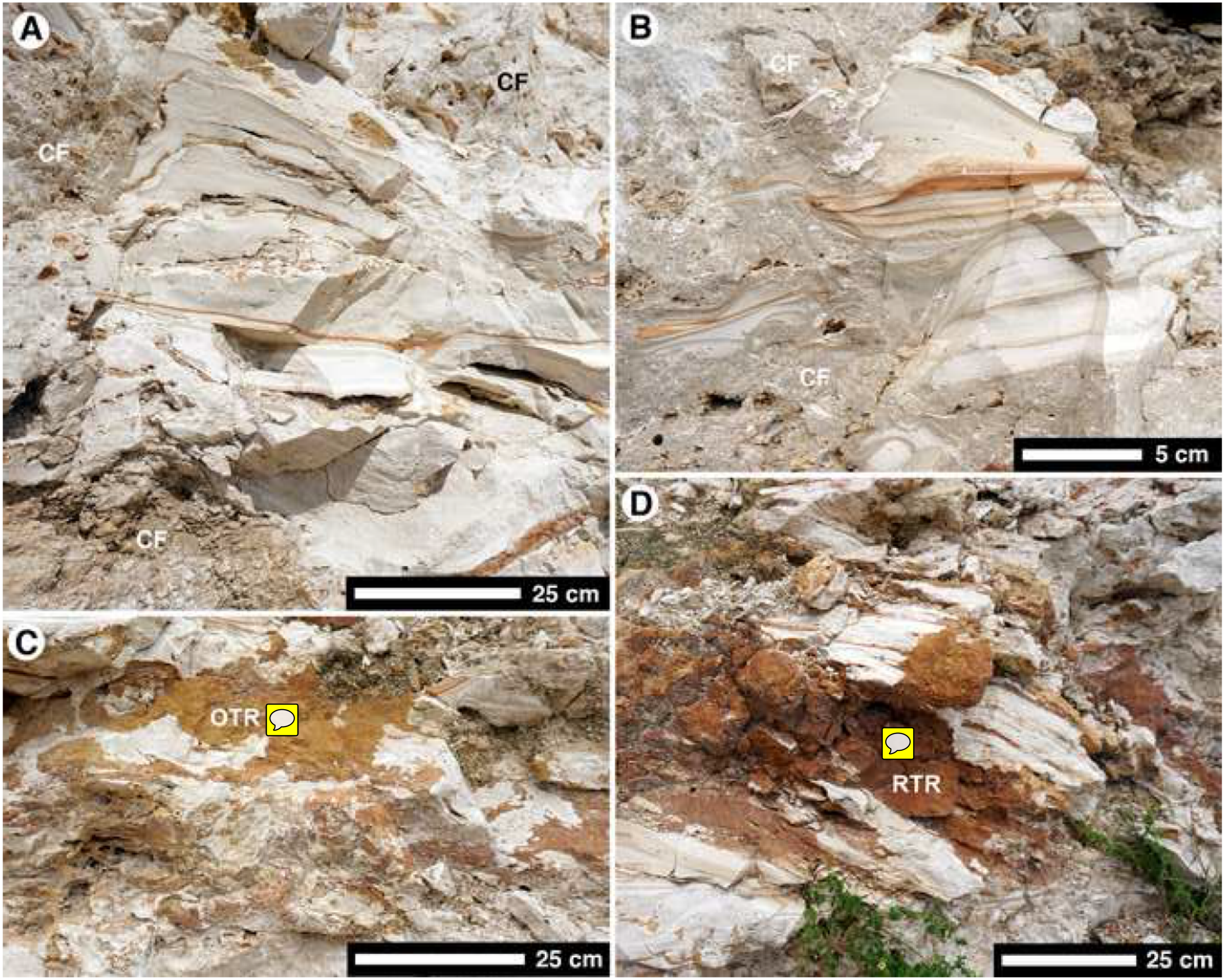

Figure 6
Click here to download high resolution image

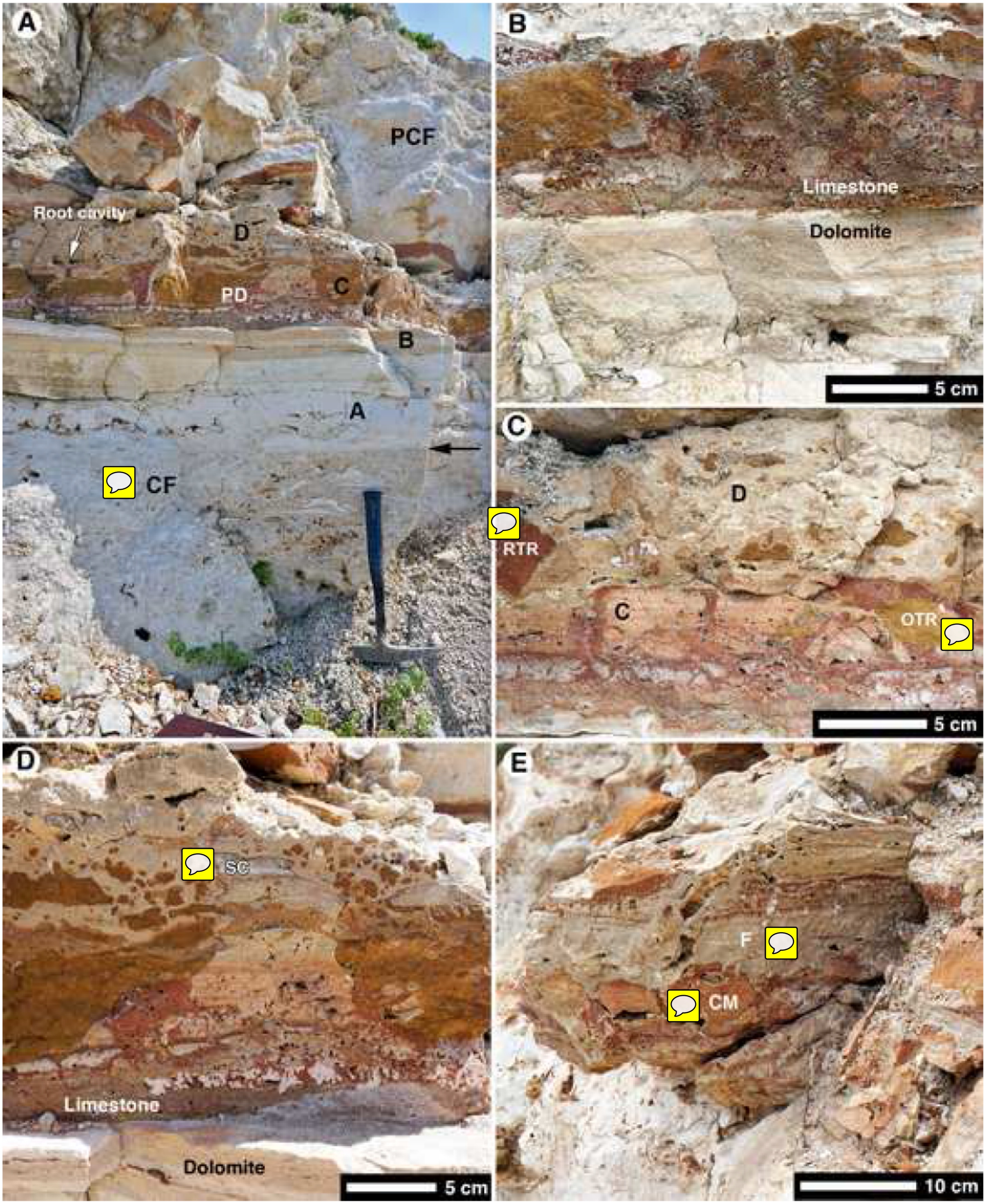

Figure 7
Click here to download high resolution image

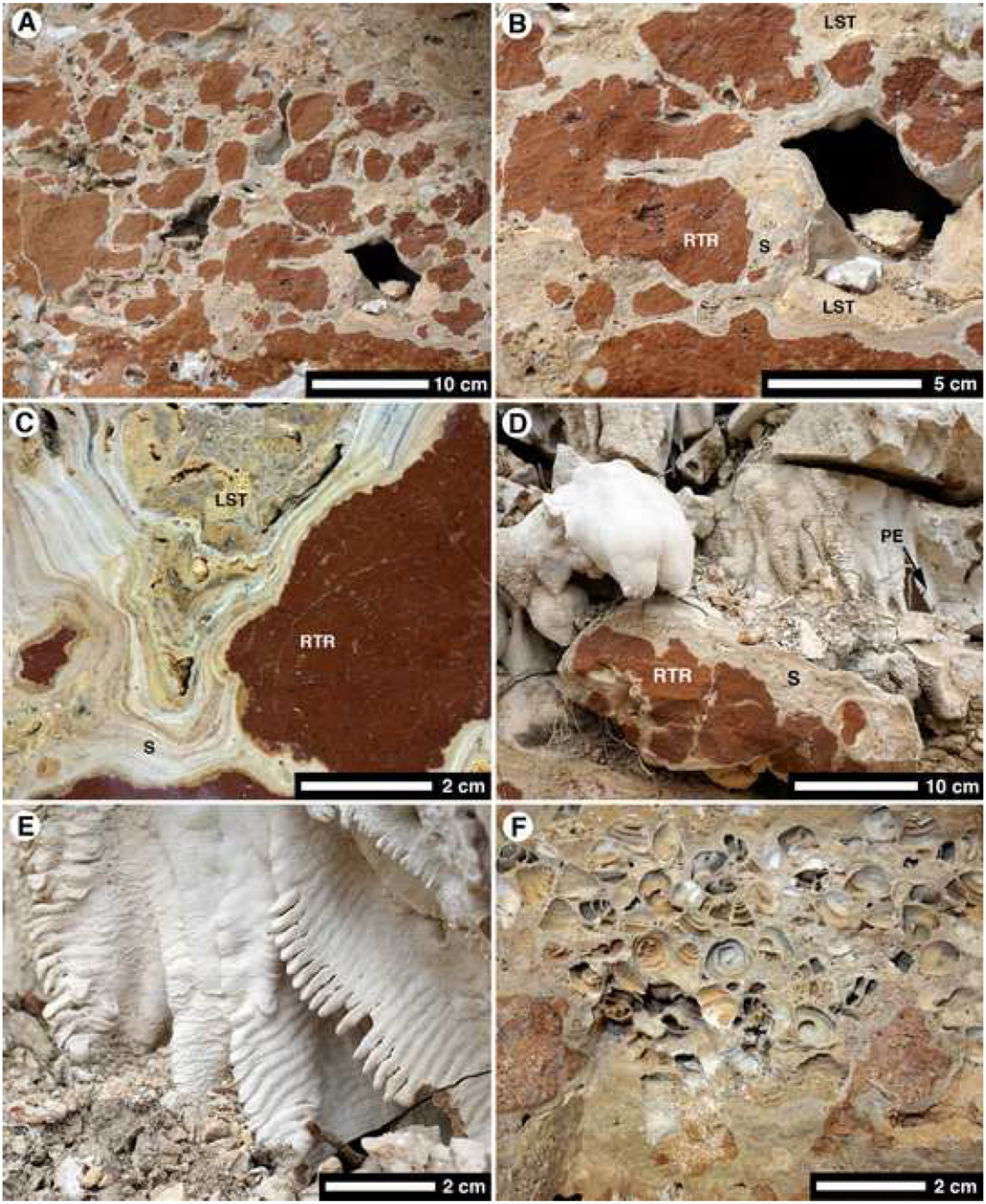

Figure 8
Click here to download high resolution image

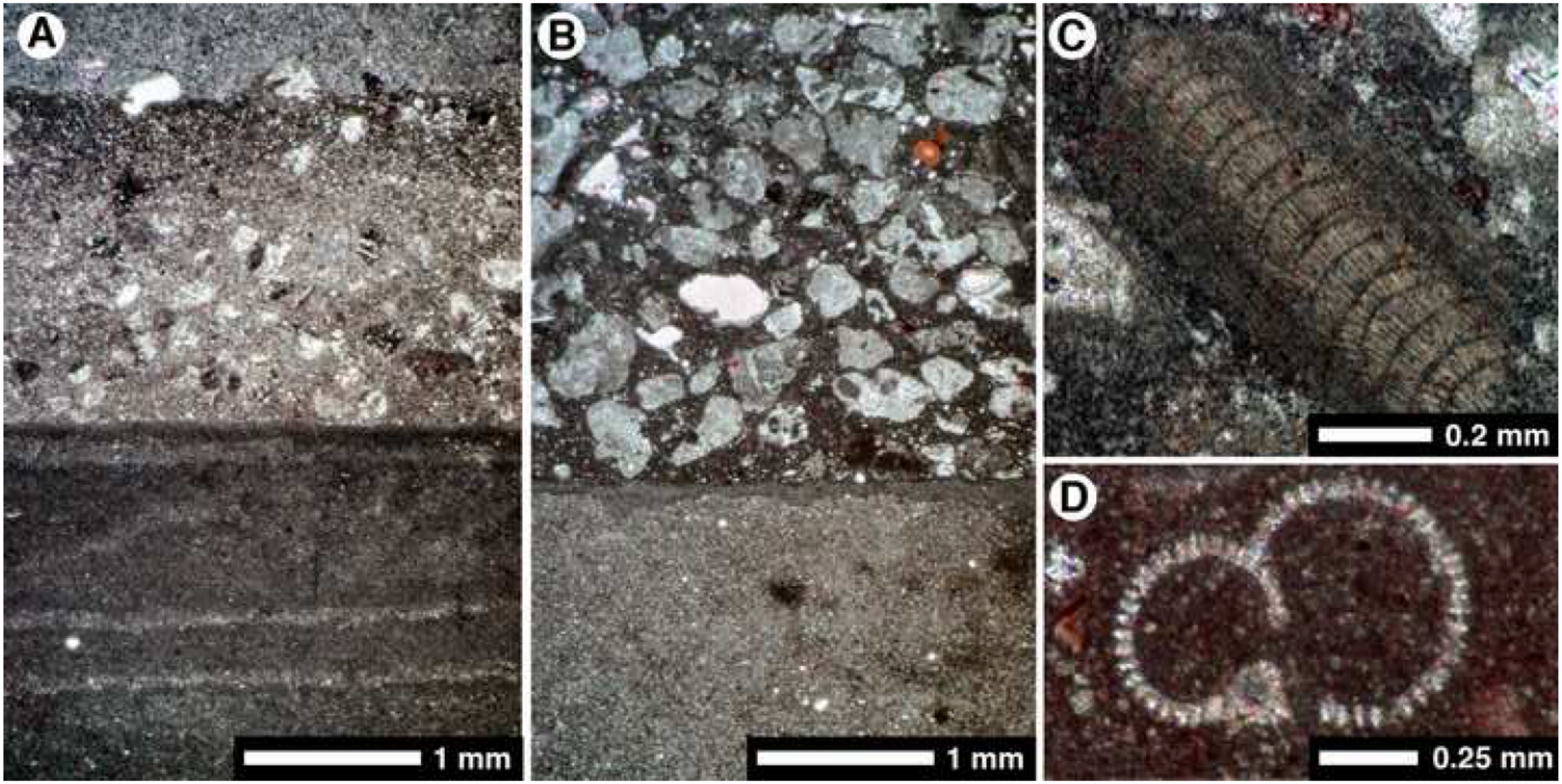

Figure 9
Click here to download high resolution image

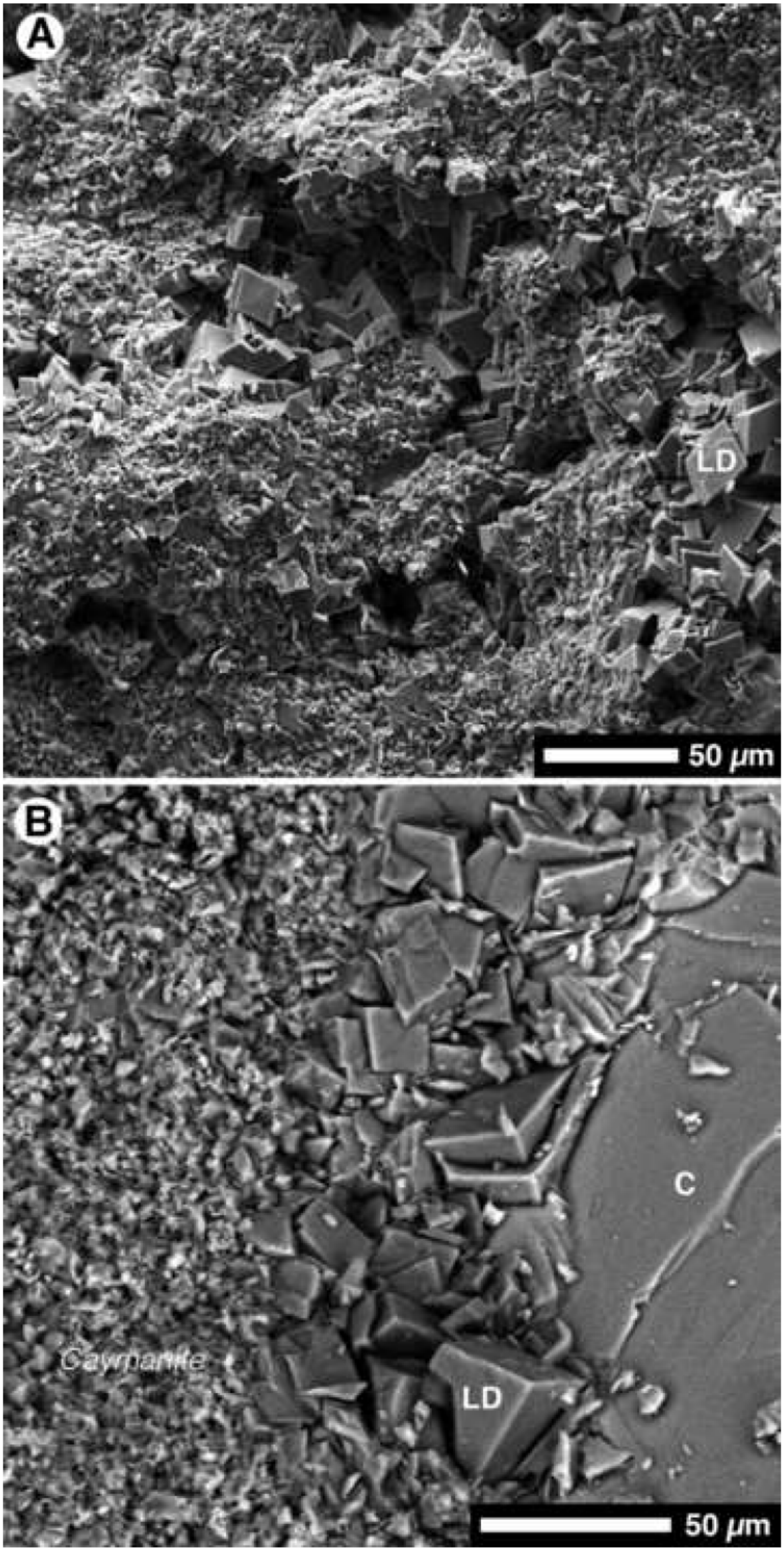

Figure 10
Click here to download high resolution image

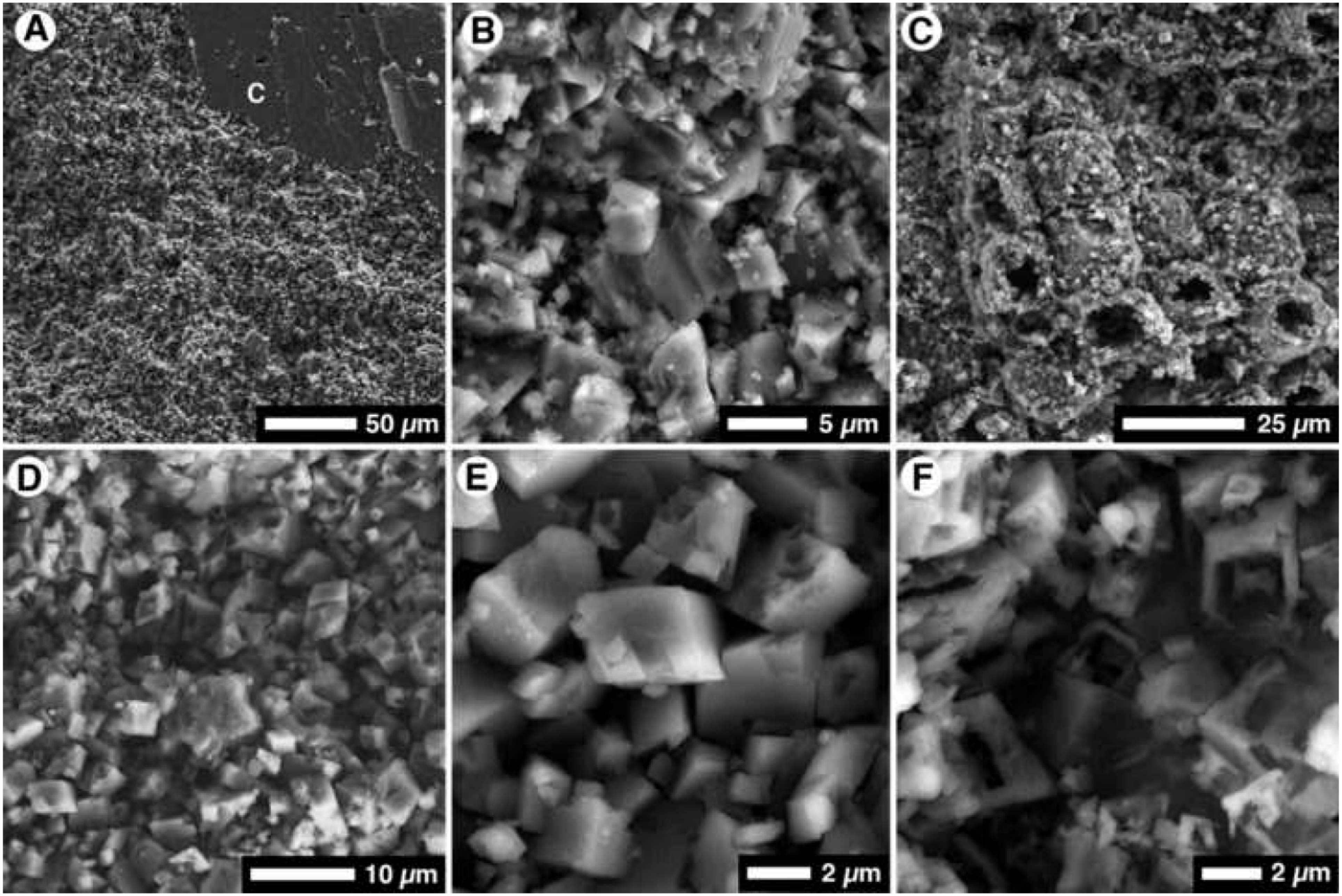

Figure 11

Click here to download high resolution image

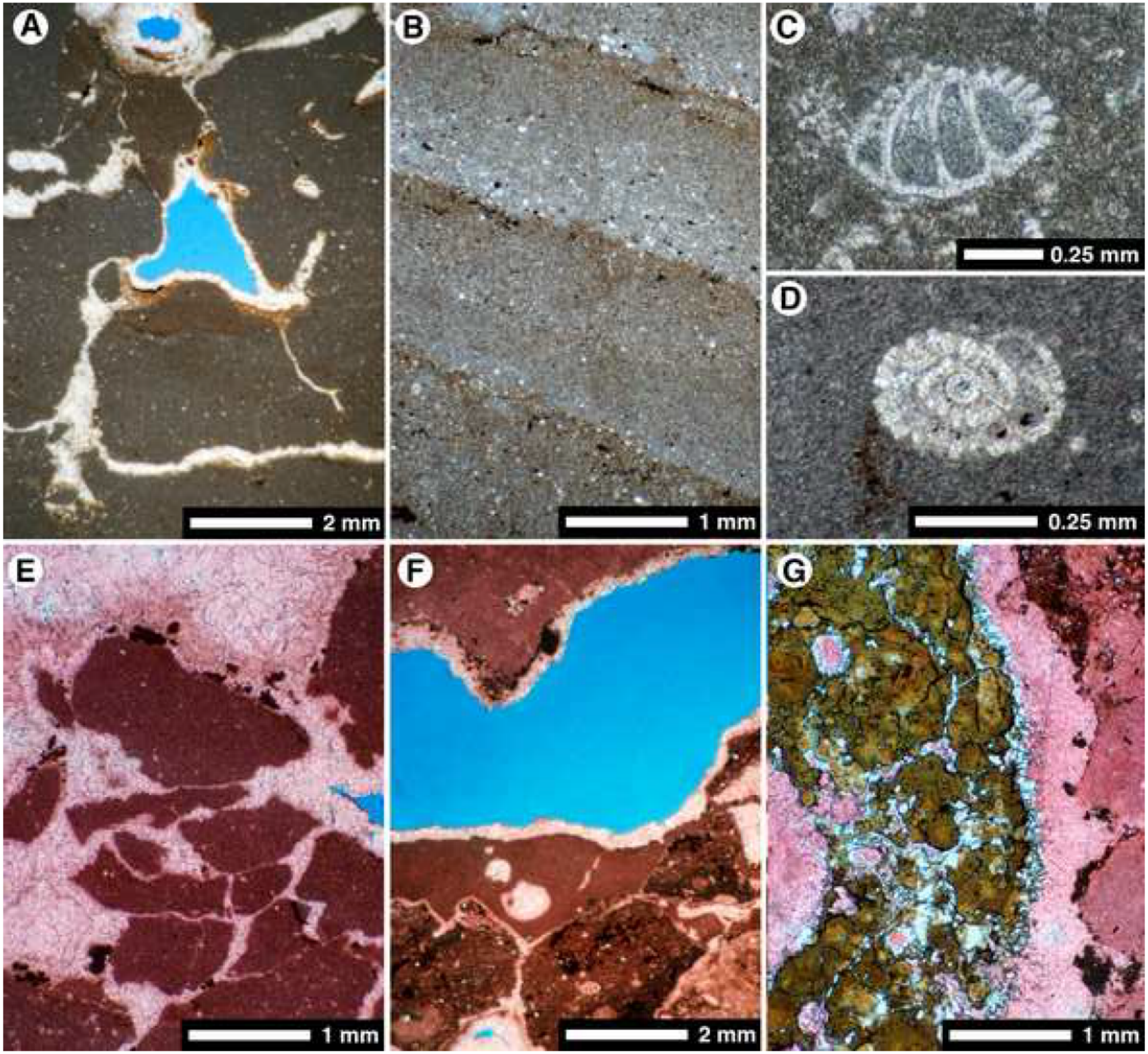

Figure 12
Click here to download high resolution image

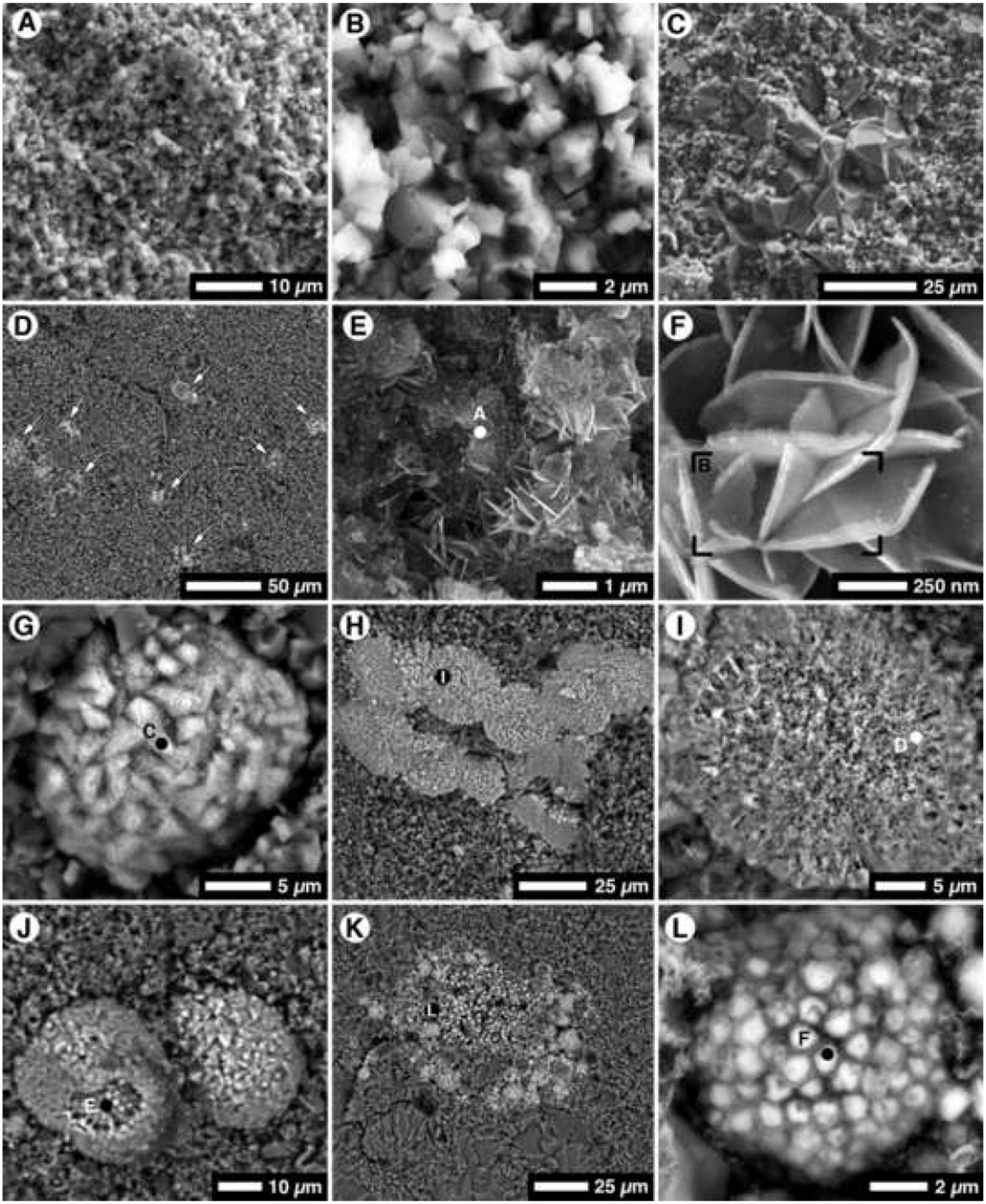

Figure 13
Click here to download high resolution image

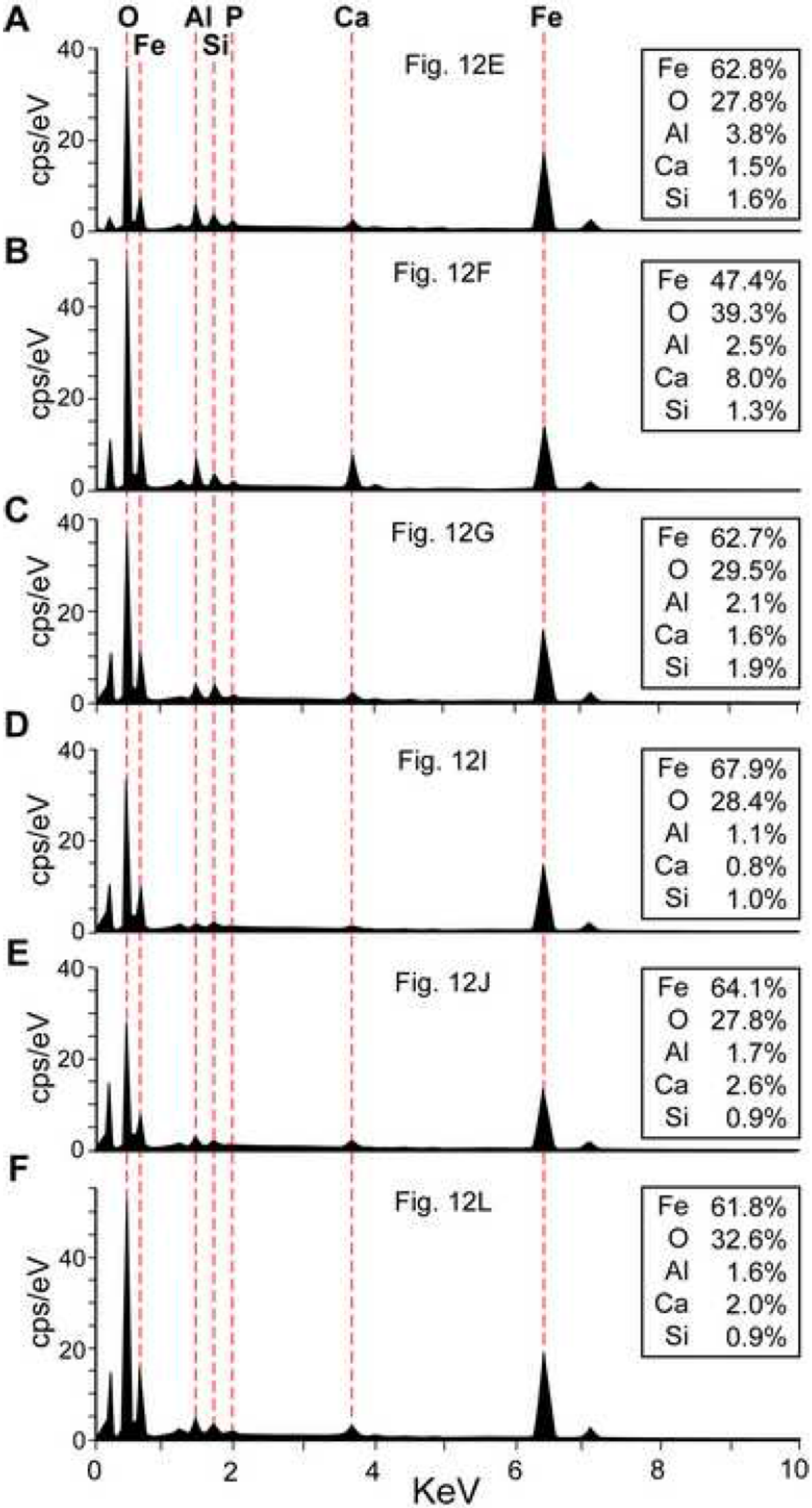

Figure 14
Click here to download high resolution image

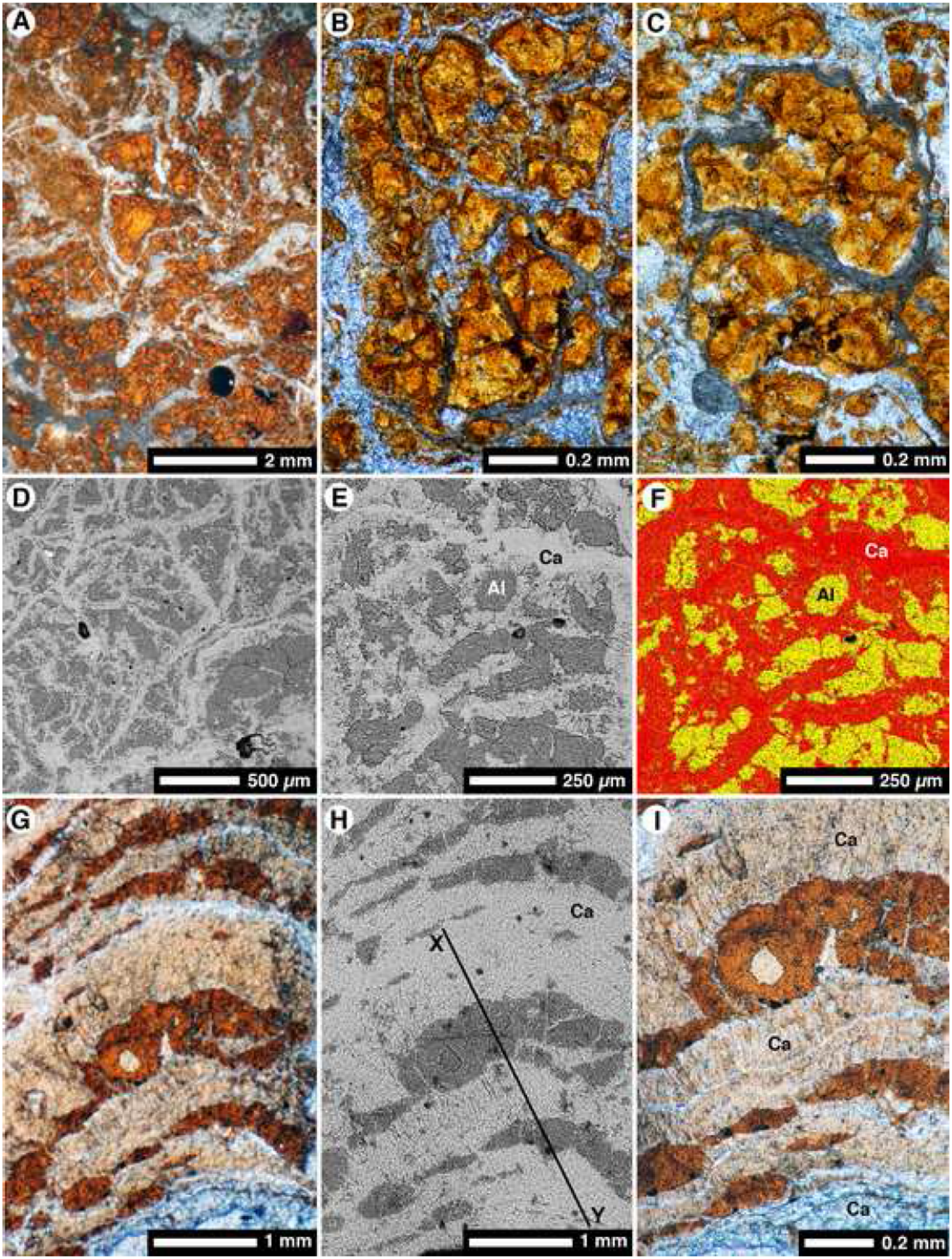

Figure 15
Click here to download high resolution image

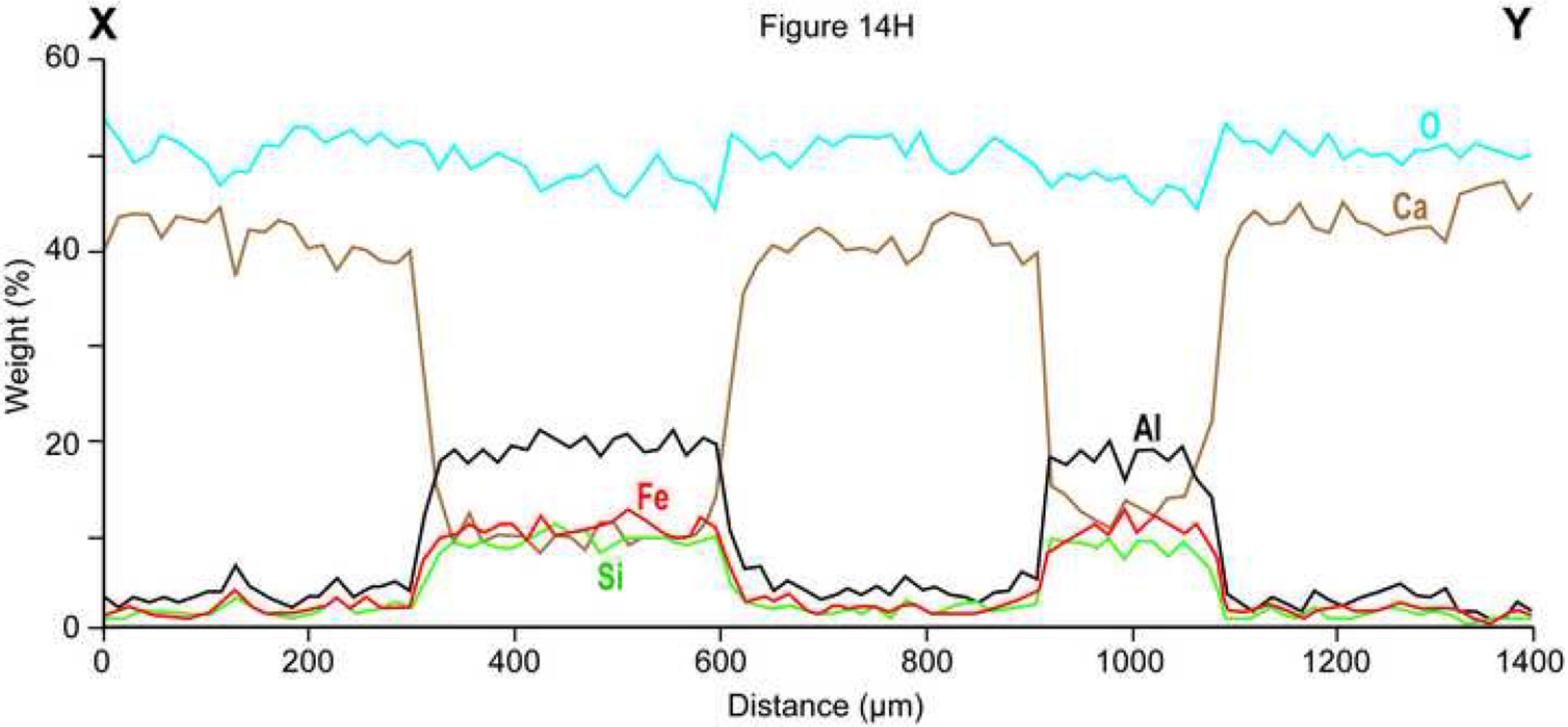

Figure 16
Click here to download high resolution image

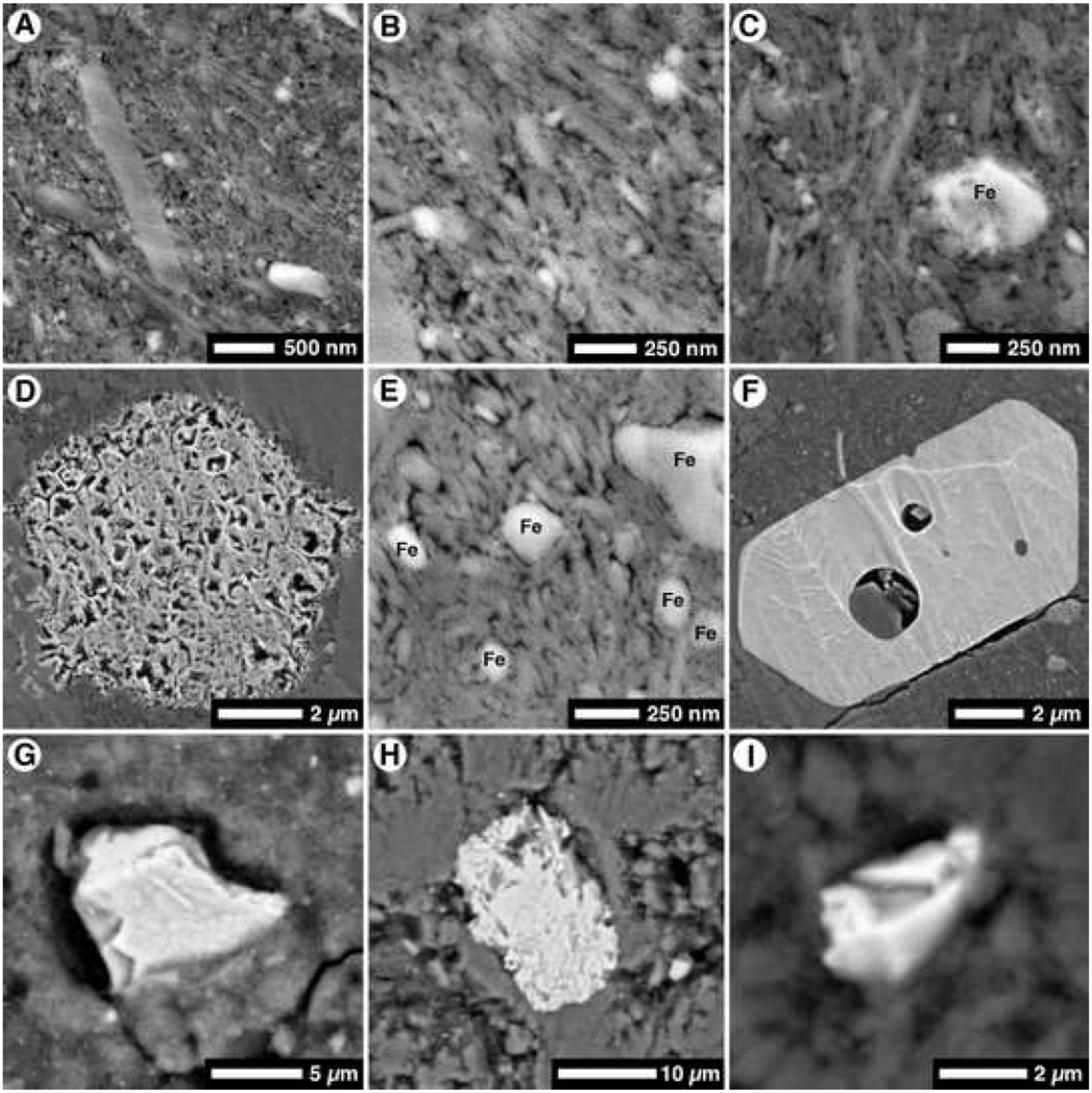

Figure 17
Click here to download high resolution image

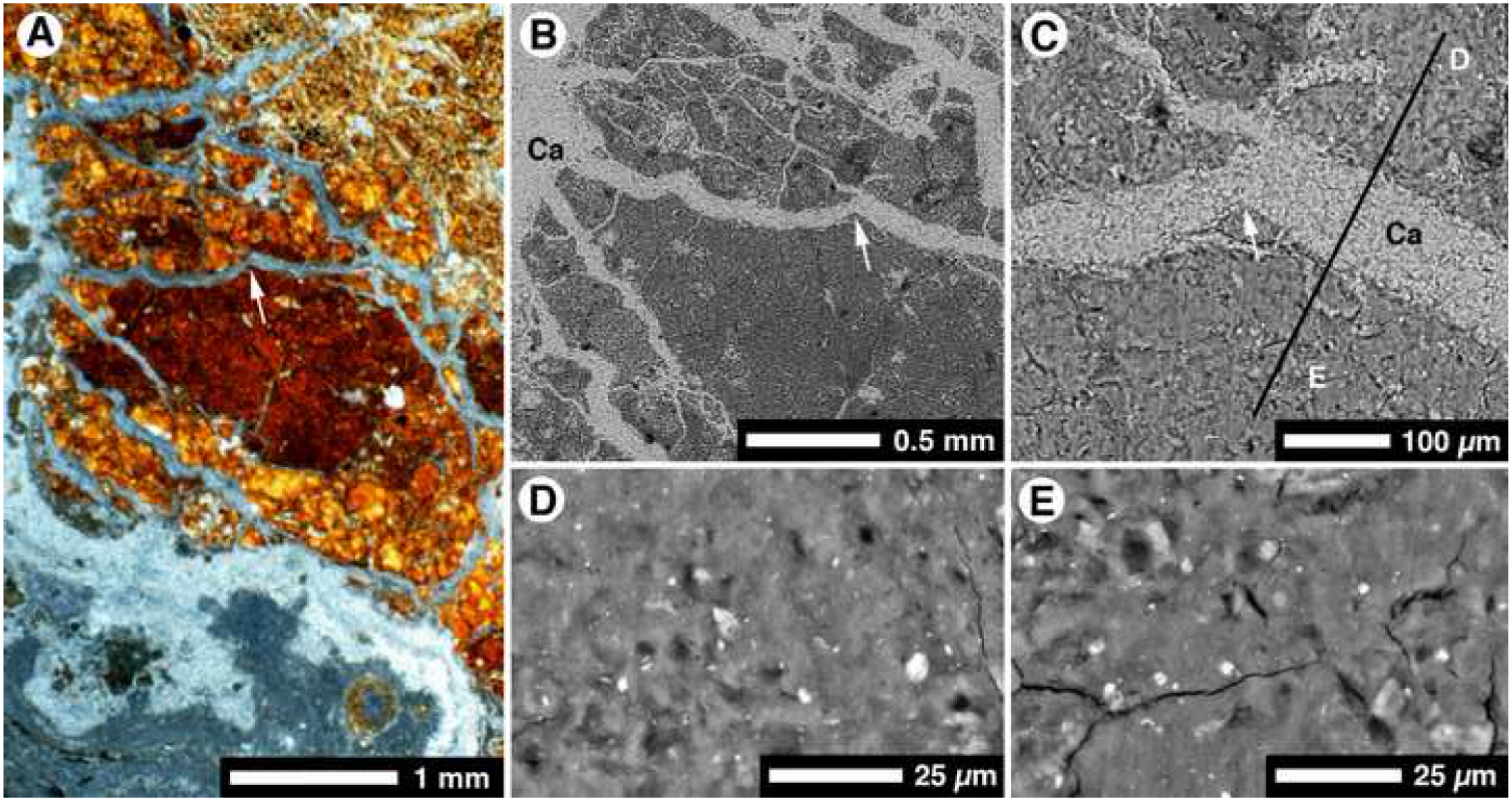

Figure 18
Click here to download high resolution image

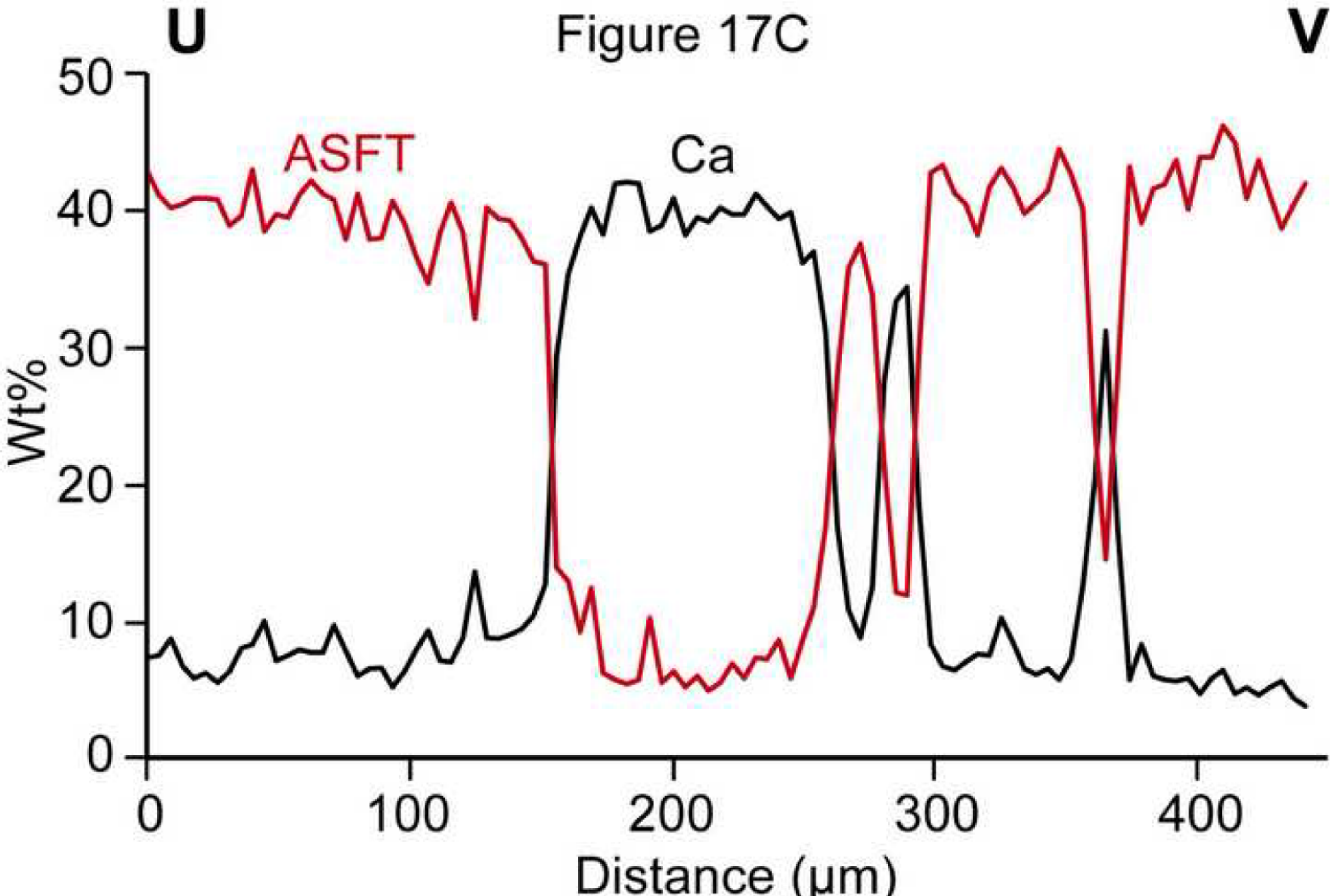

Figure 19
Click here to download high resolution image

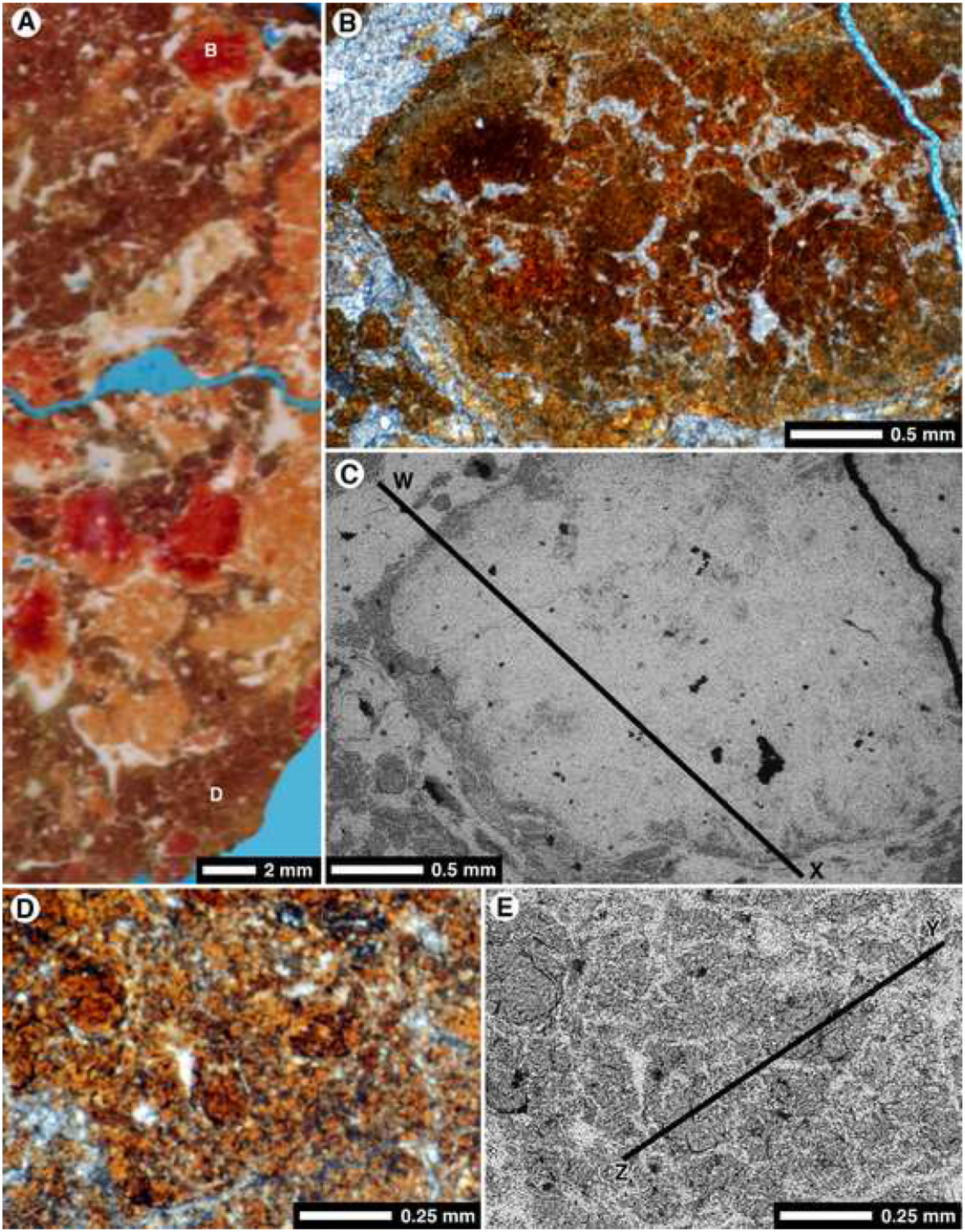

Figure 20
Click here to download high resolution image

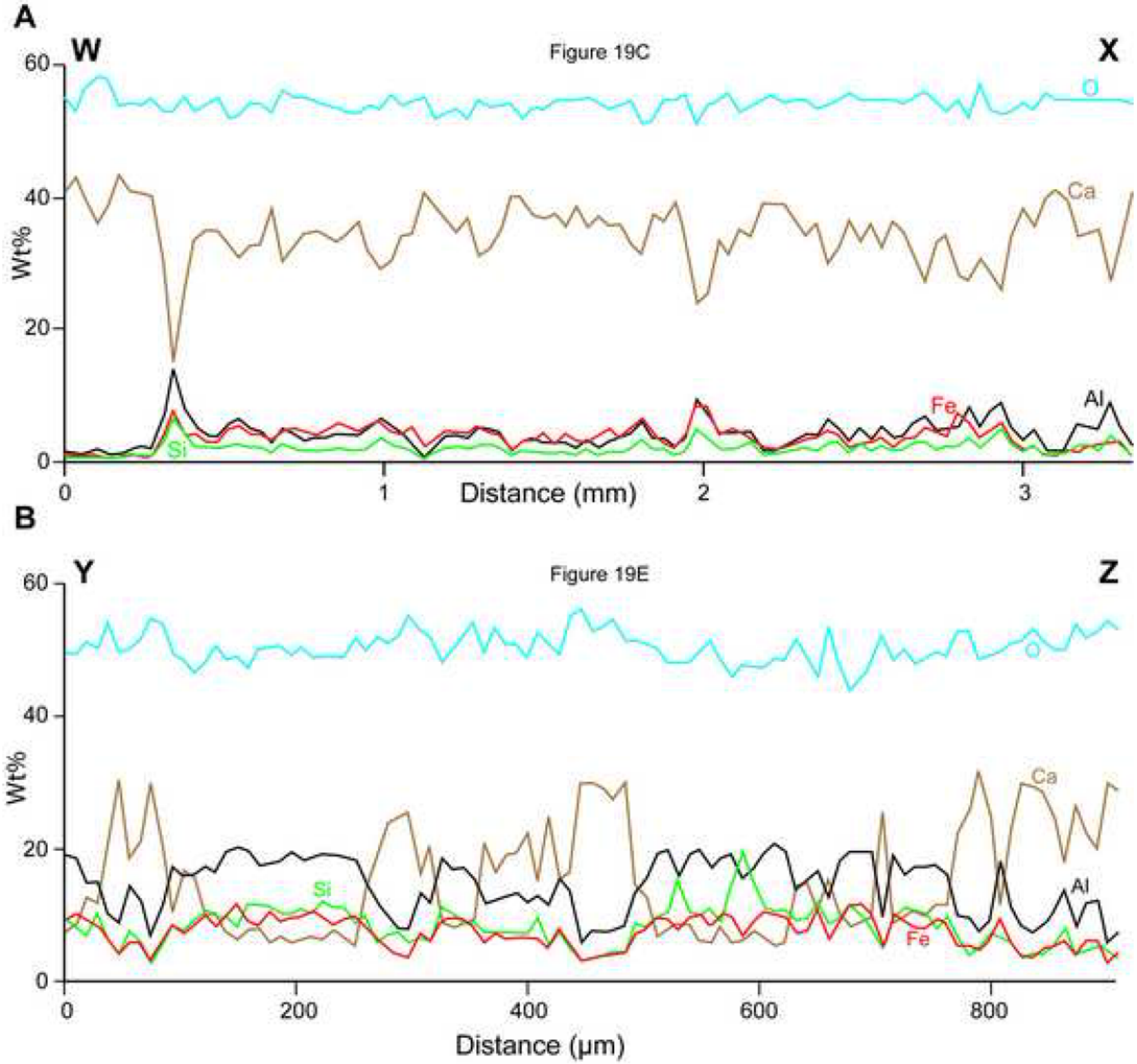

Figure 21
Click here to download high resolution image

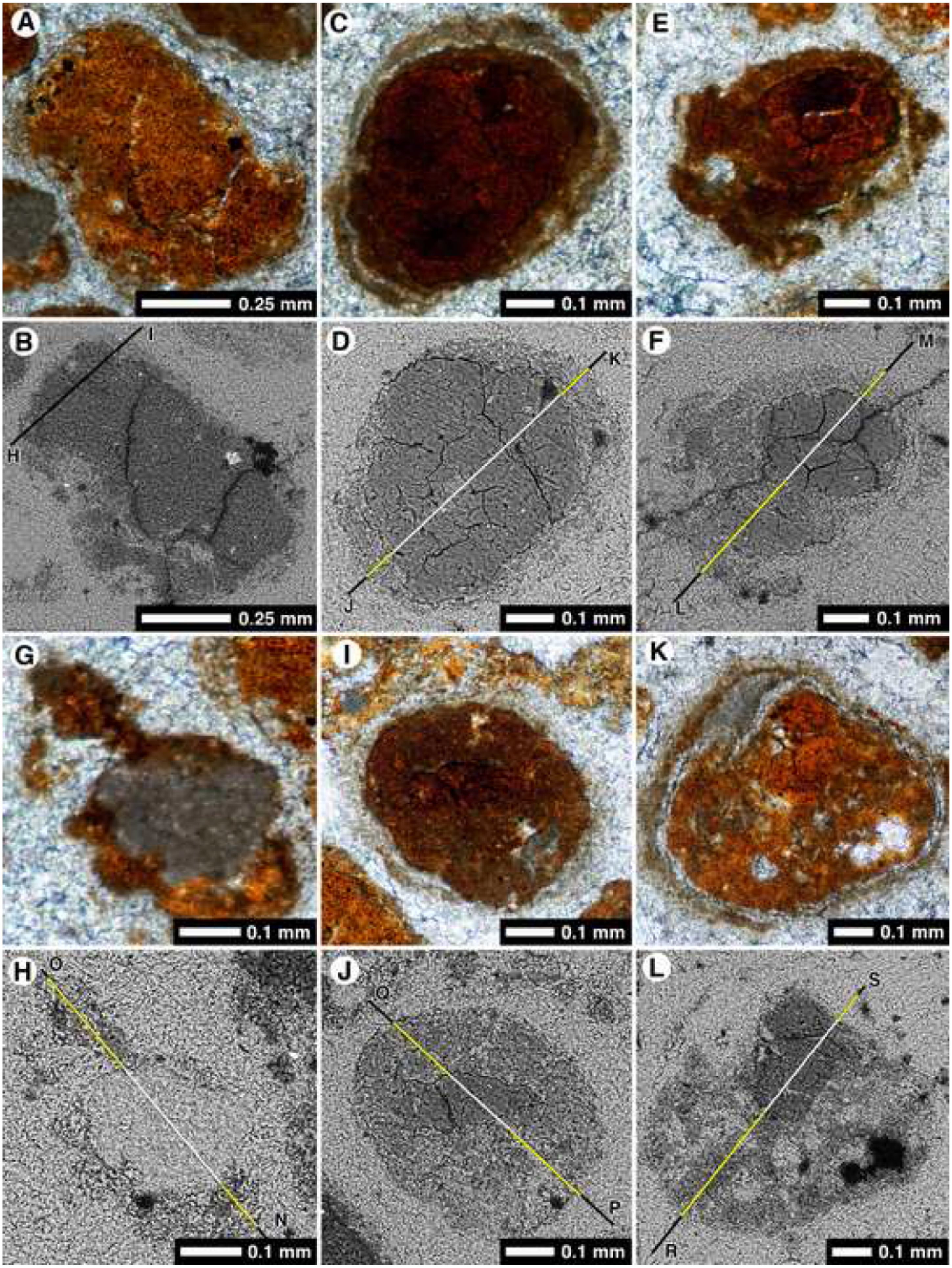

Figure 22
Click here to download high resolution image

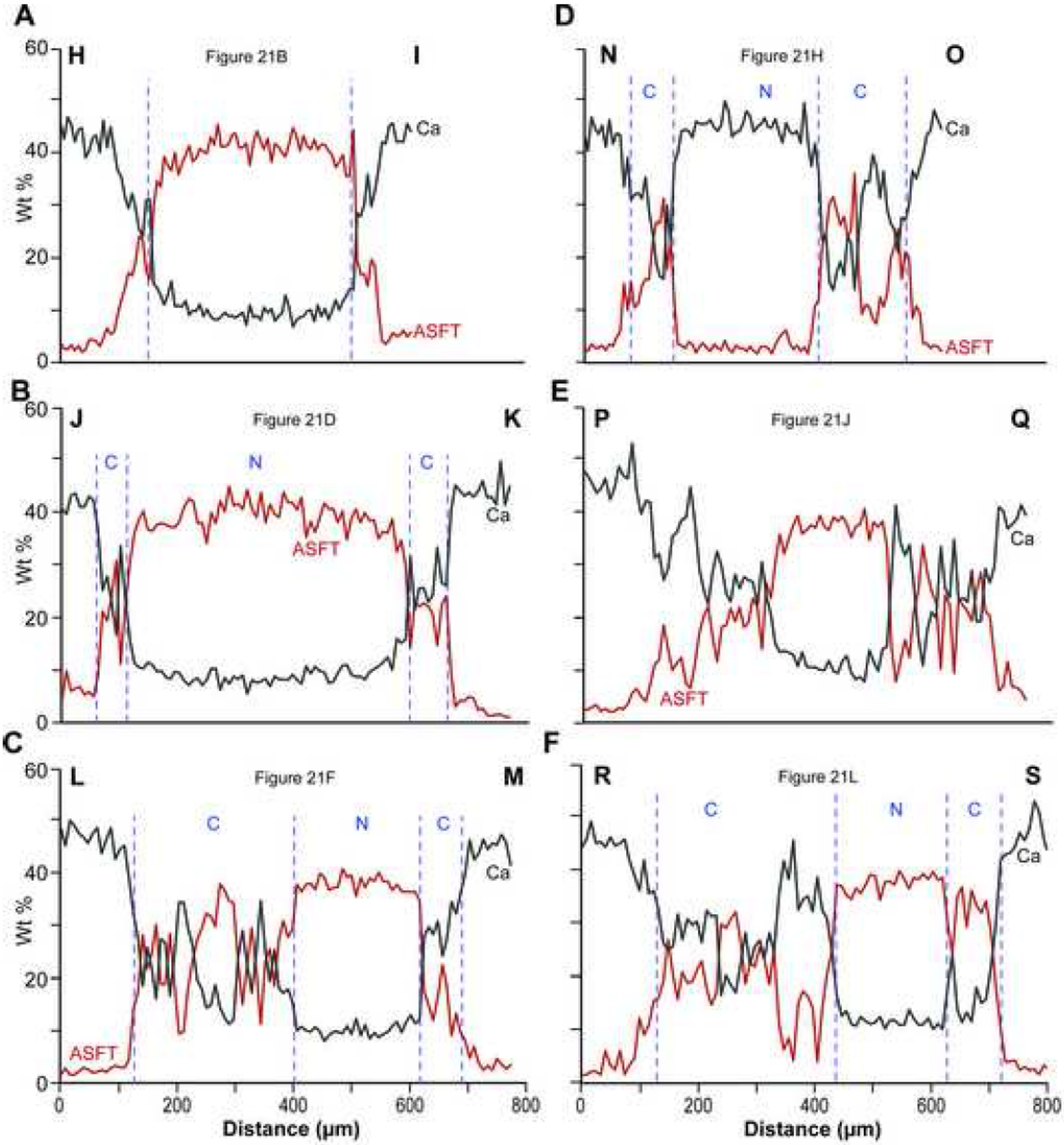

Figure 23
Click here to download high resolution image

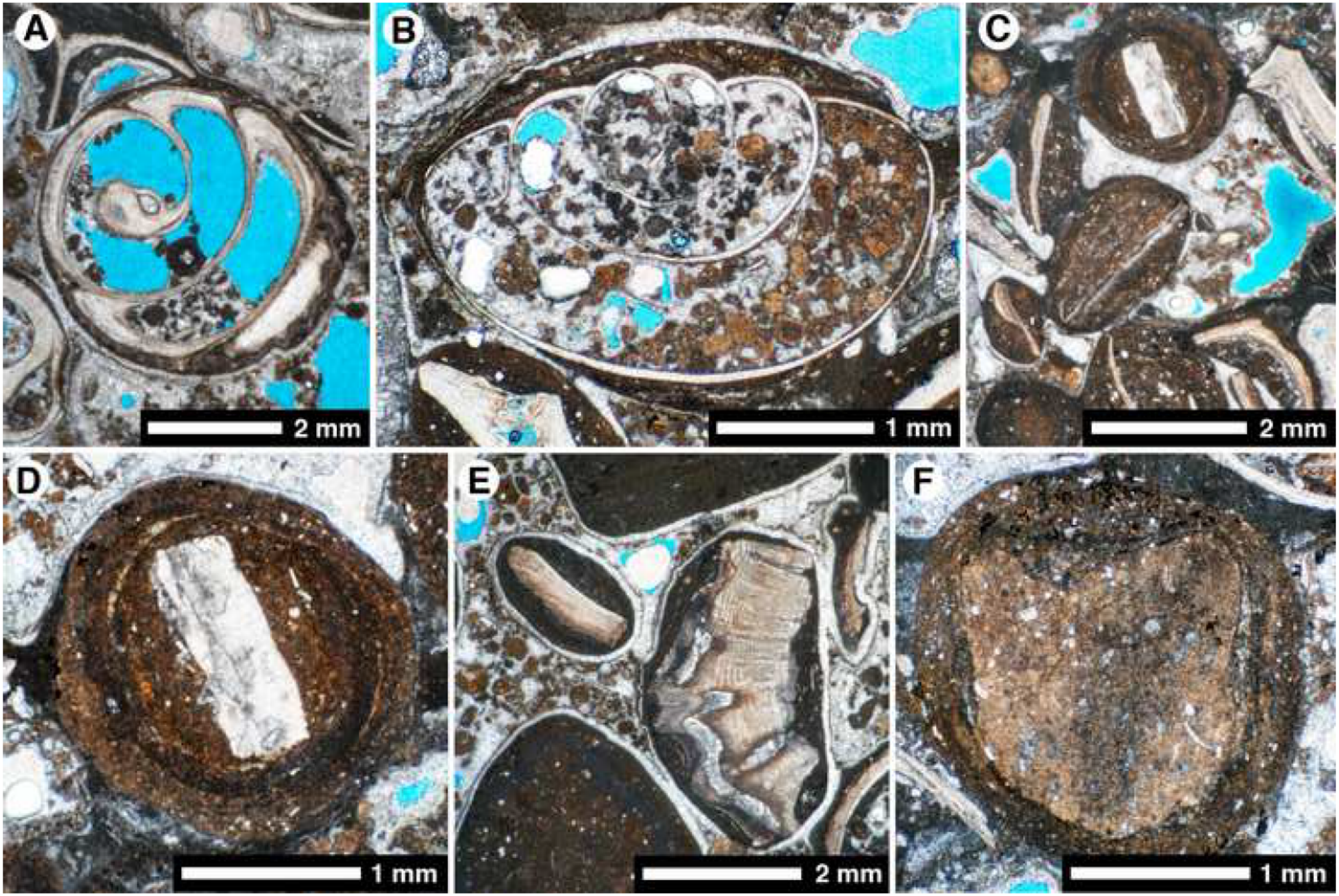

Figure 24
Click here to download high resolution image

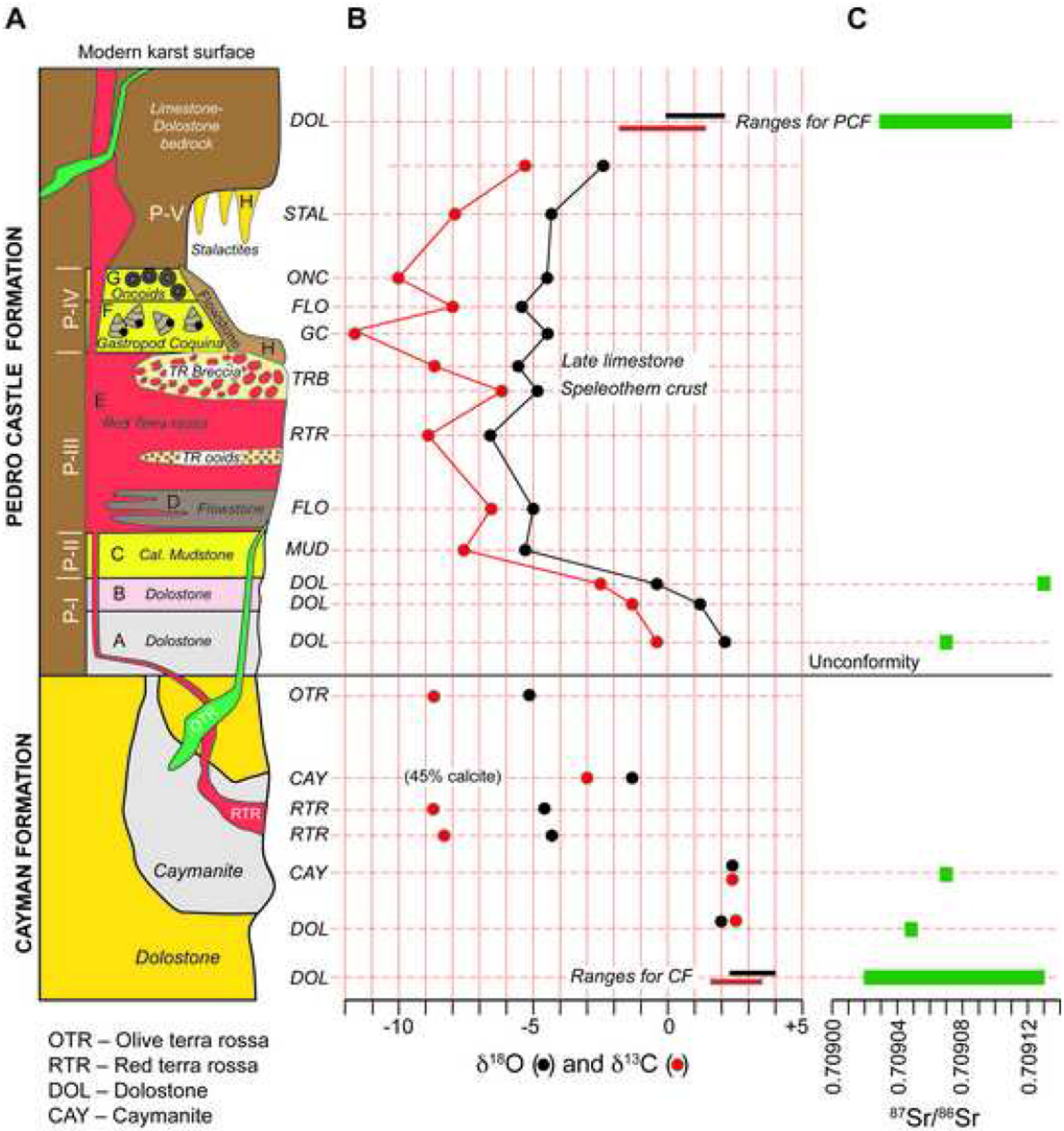

OTR – Olive terra rossa
RTR – Red terra rossa
DOL – Dolostone
CAY – Caymanite
FLO – Flowstone
MUD – Calcareous mudstone
TRB – Terra rossa breccia
GC – Gastropod coquina
ONC – Oncoid limestone
STAL – Stalactite

Figure 25

Click here to download high resolution image